AGU PUBLICATIONS

JGR

Journal of Geophysical Research: Atmospheres

RESEARCH ARTICLE
10.1002/2017JD026844

Key Points:
- New particle formation produces over half of CCN in the present-day and preindustrial atmospheres
- BVOCs are more important to CCN formation than previously thought
- Our current ion-induced nucleation rates imply only small changes of CCN over the solar cycle

Supporting Information:
- Supporting Information S1

Correspondence to:
H. Gordon,
hamish.gordon@cern.ch

Citation:
Gordon, H., et al. (2017), Causes and importance of new particle formation in the present-day and preindustrial atmospheres, *J. Geophys. Res. Atmos.*, *122*, 8739–8760, doi:10.1002/2017JD026844.

Received 24 MAR 2017
Accepted 7 JUL 2017
Accepted article online 10 JUL 2017
Published online 24 AUG 2017

Causes and importance of new particle formation in the present-day and preindustrial atmospheres

Hamish Gordon[1], Jasper Kirkby[2,3], Urs Baltensperger[4], Federico Bianchi[5], Martin Breitenlechner[6], Joachim Curtius[3], Antonio Dias[2], Josef Dommen[4], Neil M. Donahue[7], Eimear M. Dunne[8], Jonathan Duplissy[9], Sebastian Ehrhart[3,10], Richard C. Flagan[11], Carla Frege[4], Claudia Fuchs[4], Armin Hansel[12], Christopher R. Hoyle[4,13], Markku Kulmala[5], Andreas Kürten[3], Katrianne Lehtipalo[4,5], Vladimir Makhmutov[14], Ugo Molteni[4], Matti P. Rissanen[5], Yuri Stozkhov[14], Jasmin Tröstl[4], Georgios Tsagkogeorgas[15], Robert Wagner[5], Christina Williamson[16], Daniela Wimmer[5], Paul M. Winkler[17], Chao Yan[5], and Ken S. Carslaw[1]

[1]School of Earth and Environment, University of Leeds, Leeds, UK, [2]CERN, Geneva, Switzerland, [3]Institute for Atmosphere and Environment, Goethe University Frankfurt, Frankfurt, Germany, [4]Laboratory of Atmospheric Chemistry, Paul Scherrer Institute, Villigen, Switzerland, [5]Department of Physics, Division of Atmospheric Sciences, University of Helsinki, Helsinki, Finland, [6]School of Engineering and Applied Sciences, Department of Chemistry and Chemical Biology, Harvard University, Cambridge, Massachusetts, USA, [7]Center for Atmospheric Particle Studies, Carnegie Mellon University, Pittsburgh, Pennsylvania, USA, [8]Finnish Meteorological Institute, Atmospheric Research Centre of Eastern Finland, Kuopio, Finland, [9]Helsinki Institute of Physics, Helsinki, Finland, [10]Now at Atmospheric Chemistry Department, Max Planck Institute for Chemistry, Mainz, Germany, [11]Institute for Ion Physics and Applied Physics, Division of Chemistry and Chemical Engineering, California Institute of Technology, Pasadena, California, USA, [12]University of Innsbruck, Innsbruck, Austria, [13]SLFWSL Institute for Snow and Avalanche Research, Davos, Switzerland, [14]Solar and Cosmic Ray Research Laboratory, Lebedev Physical Institute, Moscow, Russia, [15]Leibniz Institute for Tropospheric Research, Leipzig, Germany, [16]Cooperative Institute for Research in Environmental Sciences, University of Colorado Boulder and National Oceanic and Atmospheric Administration Earth System Research Laboratory, Boulder, Colorado, USA, [17]Faculty of Physics, University of Vienna, Vienna, Austria

Abstract New particle formation has been estimated to produce around half of cloud-forming particles in the present-day atmosphere, via gas-to-particle conversion. Here we assess the importance of new particle formation (NPF) for both the present-day and the preindustrial atmospheres. We use a global aerosol model with parametrizations of NPF from previously published CLOUD chamber experiments involving sulfuric acid, ammonia, organic molecules, and ions. We find that NPF produces around 67% of cloud condensation nuclei at 0.2% supersaturation (CCN0.2%) at the level of low clouds in the preindustrial atmosphere (estimated uncertainty range 45–84%) and 54% in the present day (estimated uncertainty range 38–66%). Concerning causes, we find that the importance of biogenic volatile organic compounds (BVOCs) in NPF and CCN formation is greater than previously thought. Removing BVOCs and hence all secondary organic aerosol from our model reduces low-cloud-level CCN concentrations at 0.2% supersaturation by 26% in the present-day atmosphere and 41% in the preindustrial. Around three quarters of this reduction is due to the tiny fraction of the oxidation products of BVOCs that have sufficiently low volatility to be involved in NPF and early growth. Furthermore, we estimate that 40% of preindustrial CCN0.2% are formed via ion-induced NPF, compared with 27% in the present day, although we caution that the ion-induced fraction of NPF involving BVOCs is poorly measured at present. Our model suggests that the effect of changes in cosmic ray intensity on CCN is small and unlikely to be comparable to the effect of large variations in natural primary aerosol emissions.

Plain Language Summary New particle formation in the atmosphere is the process by which gas molecules collide and stick together to form atmospheric aerosol particles. Aerosols act as seeds for cloud droplets, so the concentration of aerosols in the atmosphere affects the properties of clouds. It is important to understand how aerosols affect clouds because they reflect a lot of incoming solar radiation away from Earth's surface, so changes in cloud properties can affect the climate. Before the Industrial Revolution,

aerosol concentrations were significantly lower than they are today. In this article, we show using global model simulations that new particle formation was a more important mechanism for aerosol production than it is now. We also study the importance of gases emitted by vegetation, and of atmospheric ions made by radon gas or cosmic rays, in preindustrial aerosol formation. We find that the contribution of ions and vegetation to new particle formation was also greater in the preindustrial period than it is today. However, the effect on particle formation of variations in ion concentration due to changes in the intensity of cosmic rays reaching Earth was small.

1. Introduction

Atmospheric aerosol particles play a key role in regulating Earth's radiative balance. Anthropogenic changes in aerosols have led to a significant but poorly quantified negative forcing of climate over the industrial period. To better quantify this negative forcing, an improved understanding of preindustrial aerosol is needed [*Carslaw et al.*, 2017]. New particle formation (NPF) is well established as the source of around half of cloud-forming particles in the present-day atmosphere [*Merikanto et al.*, 2009; *Wang and Penner*, 2009; *Yu and Luo*, 2009; *Pierce and Adams*, 2009a]. However, the role of NPF in the preindustrial atmosphere is less well understood. This is especially important since preindustrial aerosol concentrations were almost certainly more sensitive to changes in primary aerosol emissions and new particle formation rates than they are today [*Jones et al.*, 1994; *Carslaw et al.*, 2013], and the preindustrial atmosphere forms a highly uncertain baseline from which aerosol-cloud radiative forcing is calculated.

Here we study the role of NPF in the present-day and preindustrial atmospheres using a global aerosol model. We quantify its importance by calculating the fraction of global cloud condensation nuclei (CCN) number concentrations that originate from NPF, approximated by the change in CCN that results when NPF is removed from the model. This quantity has been calculated before for the present-day atmosphere [*Spracklen et al.*, 2008; *Merikanto et al.*, 2009; *Yu and Luo*, 2009], and the influence of NPF on cloud droplet numbers and forcing has also been estimated [*Merikanto et al.*, 2010; *Kazil et al.*, 2010; *Wang and Penner*, 2009; *Makkonen et al.*, 2009]. However, while there are studies of the impact of different NPF mechanisms, such as boundary layer particle formation [*Merikanto et al.*, 2010; *Pierce and Adams*, 2009a] on the preindustrial atmosphere, we are not aware of any previous estimates of the role of NPF in cloud-level CCN formation in this environment.

Our understanding of NPF has improved substantially in the last 10 years. These recent developments permit us to estimate the state of the preindustrial atmosphere more reliably and also motivate an update to studies of the present day. Since previous publications [*Merikanto et al.*, 2009; *Wang and Penner*, 2009; *Yu and Luo*, 2009], instrumentation such as time-of-flight mass spectrometry has been made sufficiently sensitive to measure NPF directly in the field and in the laboratory [e.g., *Wyche et al.*, 2007; *Junninen et al.*, 2010]. These instruments can now identify the kinds of molecules in the smallest nucleating clusters [e.g., *Bianchi et al.*, 2016; *Schobesberger et al.*, 2013], and when coupled to more advanced particle detection instruments [e.g., *Iida et al.*, 2009; *Vanhanen et al.*, 2011], we can now make more accurate NPF rate measurements [e.g., *Kürten et al.*, 2016; *Kontkanen et al.*, 2017]. Laboratory experiments are important for separating the compounds that participate in nucleation. Some recent chamber studies focused on NPF involving sulfuric acid and water alone [e.g., *Zollner et al.*, 2012; *Duplissy et al.*, 2016], or sulfuric acid with ammonia [e.g., *Benson et al.*, 2011; *Kürten et al.*, 2016]. Furthermore, NPF rates of sulfuric acid with amines [*Almeida et al.*, 2013; *Jen et al.*, 2014] or organic compounds [*Metzger et al.*, 2010; *Riccobono et al.*, 2014] and of organic compounds alone [*Kirkby et al.*, 2016] have now also been measured in the laboratory. Better mathematical models for the molecular clustering process have also been published recently, for example, by *Chen et al.* [2012].

These developments have permitted global model studies to simulate the roles of diverse compounds, most notably ammonia and monoterpene oxidation products, in NPF alongside sulfuric acid. Including these compounds has a considerable effect on simulations of CCN concentrations, particularly in the preindustrial atmosphere where sulfuric acid emissions were much lower [*Dentener et al.*, 2006] but monoterpene concentrations, globally averaged, were relatively similar [*Acosta Navarro et al.*, 2014]. In the GLOMAP model, for example, the increase in surface-level CCN concentrations at 0.2% supersaturation (hereafter CCN0.2%) over the industrial period is 102% when organic compounds do not participate in NPF [*Scott et al.*, 2014]. When *Gordon et al.* [2016] added the NPF of pure organic particles and organic particles with H_2SO_4 from CLOUD chamber measurements [*Kirkby et al.*, 2016; *Riccobono et al.*, 2014], the 102% increase in CCN concentrations over the industrial period was reduced to 60%. There is considerable diversity among model estimates

of these changes, mainly due to uncertainties in the preindustrial baseline: for example, the corresponding increase calculated by *Pierce and Adams* [2009a] using the GISS-TOMAS model (without organic compounds participating in nucleation) was 220%.

In the current study, we combine for the first time the parametrization of ion-induced NPF of monoterpene oxidation products alone [*Kirkby et al.*, 2016] with the NPF model presented by *Dunne et al.* [2016], which quantifies NPF in terms of sulfuric acid, ions, ammonia, and monoterpene oxidation products [*Riccobono et al.*, 2014] throughout the troposphere. We describe the model then present the role of NPF in CCN formation and discuss our uncertainties. The model used is similar to previous studies, but a limited reevaluation of simulated CCN concentrations is presented in supporting information Text S2. With this updated model we perform two additional studies, which we now introduce.

The results of *Carslaw et al.* [2013] suggest that any link between cosmic rays and climate via NPF should be stronger in the preindustrial atmosphere, when the sensitivity of CCN concentrations to external perturbations was higher. Several previous model studies of the present-day atmosphere found that variations in the cosmic ray intensity typical of the solar cycle were very unlikely to produce significant variations in CCN concentrations [*Pierce and Adams*, 2009b; *Snow-Kropla et al.*, 2011; *Yu et al.*, 2012; *Dunne et al.*, 2012; *Kazil et al.*, 2012; *Yu and Luo*, 2014a]. We update these studies with our improved NPF model, and we explore possible effects in both preindustrial and present-day conditions.

The increased importance of the oxidation products of biogenic volatile organic compounds (BVOCs) in our model compared to previous work leads us to update our estimate of their role in preindustrial and present-day CCN formation. The previously referenced study by *Scott et al.* [2014] showed that CCN concentrations are sensitive to organic NPF mechanisms. When BVOCs participated in NPF, adding them to a simulation of the present-day atmosphere where they had previously been switched off increased CCN0.2% concentrations by 45%, while when they do not participate in NPF, the corresponding increase in CCN0.2% was only around 10%. We repeat these estimates with our updated NPF model and also propose an alternative calculation of the importance of BVOCs in CCN formation.

2. Global Aerosol Model

We use the global aerosol model GLOMAP [*Spracklen et al.*, 2005] to simulate CCN concentrations, starting from NPF or primary particulate emissions as in *Merikanto et al.* [2009]. The model resolution is $2.8^\circ \times 2.8^\circ$ horizontally, and there are 31 vertical hybrid sigma-pressure levels from ground level to 10 hPa. GLOMAP is embedded within a chemical transport model, TOMCAT [*Chipperfield*, 2006], and simulates the formation, growth, coagulation, advection, cloud processing, and deposition of aerosol. Early model versions used a sectional representation of the aerosol size distribution, but the version we use here simulates the aerosol in seven lognormal size modes, as described by *Mann et al.* [2010]. The model we use here is almost identical to that used in a detailed comparison with the sectional model [*Mann et al.*, 2012]. Four of the modes (nucleation, Aitken, accumulation, and coarse) are hydrophilic, and there are also hydrophobic Aitken, accumulation, and coarse modes. The composition of each mode is determined by the relative fractions of the sulfate, sea-salt, black carbon, and organic carbon compounds. Dust is not included, as it was not found to contribute significantly to CCN by *Manktelow et al.* [2009], and we also confirmed that omitting it does not affect our results significantly. Meteorology is forced by fields from the European Centre for Medium-Range Weather Forecasting. CCN concentrations are calculated with the method of *Petters and Kreidenweis* [2007], assuming, from Table 1 in their article, hygroscopicities κ of 0.61 for sulfate, 1.28 for sea salt, 0.1 for organic carbon, and zero for black carbon.

Primary emissions of black and organic carbon from biofuel and fossil fuel burning, and of sulfur dioxide, are read in from the AeroCom database for the years 2000 and 1750 [*Dentener et al.*, 2006]. Fire emissions are taken from the GFED inventory, version 1, averaged between 1997 and 2002 [*Van Der Werf et al.*, 2003] for both preindustrial and present day. The mode diameter of biofuel and biomass burning particles is assumed to be 150 nm and that of fossil fuel burning emissions 60 nm [after *Stier et al.*, 2005]. The standard deviation of the lognormal modes is 1.59. The distribution of these primary particles is then incorporated into the insoluble Aitken mode. Primary emissions of sea salt are calculated using parametrizations by *Mårtensson et al.* [2003] below 2 μm particle diameter and *Monahan et al.* [1986] above. Compared to a parametrization by *Gong* [2003] used in previous model versions, the total particle number is substantially increased in the Southern Ocean by the inclusion of the Mårtensson scheme, which represents ultrafine sea salt and is in better agreement

with more recent studies [*de Leeuw et al.*, 2011]. We further assume 2.5% of emitted SO_2 vapor mass is emitted as primary sulfate particles, following AeroCom recommendations [*Stier et al.*, 2005].

Emissions of dimethyl sulfide (DMS) are represented using the scheme of *Kettle and Andreae* [2000] and assumed to be the same in preindustrial and present-day simulations. The oxidant concentrations (ozone, OH, and NO_3) are read in every 6 h from dedicated TOMCAT simulations of the preindustrial and present-day atmospheres, both including isoprene. The oxidants react with SO_2 and monoterpenes (at the reaction rates for α-pinene) to produce sulfuric acid and, with a 13% yield, a gaseous oxidized organic proxy. These vapors condense onto all particles at the kinetic limit. The production rate of secondary organic aerosol that results is 14.2 Tg C yr^{-1}. Ammonia emissions from the EDGAR inventory are used to determine concentration fields in a dedicated TOMCAT model run employing the hybrid dissolution solver HyDiS-1.0 [*Benduhn et al.*, 2016; *Dunne et al.*, 2016]. These fields are then read into the GLOMAP model to determine ternary inorganic NPF rates.

Ions are introduced to the model to simulate ion-induced NPF [*Dunne et al.*, 2016]. At the surface over land, most ions come from radon decay, which is included using data provided by *Zhang et al.* [2011]. Above the surface and over the ocean, ionization by cosmic rays is more important. The ionization rates from cosmic rays are calculated from lookup tables [*Usoskin et al.*, 2005, 2011] which are provided for solar cycles from 1952 to 2009, so the effect of the Sun's magnetic field can be incorporated via the heliospheric modulation potential. The technique of *Fraser-Smith* [1987] is used to calculate the geomagnetic cutoff rigidity from the International Geomagnetic Reference Field (IGRF) coefficients [*Finlay et al.*, 2010]. These coefficients are available with 5-yearly time resolution so are interpolated within the 5 year periods, while the atmospheric depth (which determines the interaction probability of a cosmic ray) and the heliospheric modulation potential are spatially interpolated across the model grid boxes. The ion concentrations [n] are calculated from the ion production rate assuming that the main loss processes for ions are ion-ion recombination and the condensation sink of ions to preexisting particles greater than 3 nm in diameter, as described (in the supporting information) by *Dunne et al.* [2016]. The solar cycle in the preindustrial simulations is assumed to be the same as in the present-day, as we do not have the modulation potentials or IGRF coefficients for 1750.

The NPF rates in our model are based on CLOUD chamber measurements. In this paper, we start from the model for NPF used in the global modeling study of *Dunne et al.* [2016]. Fuller descriptions of the NPF rate measurements in this model were published by *Riccobono et al.* [2014], *Duplissy et al.* [2016], and *Kürten et al.* [2016]. We then add the parametrization of organic NPF without sulfuric acid published by *Kirkby et al.* [2016] and used in one previous modeling study [*Gordon et al.*, 2016].

In our model, inorganic NPF involves sulfuric acid, ammonia, and ions. The NPF rate is expressed as the sum of "binary" sulfuric acid-water NPF and "ternary" sulfuric acid-ammonia-water components. New particle formation involving iodine oxides or amines is not considered here, but the potential importance of amines in global aerosol formation was studied by *Yu and Luo* [2014b] in depth, and a sensitivity study with the GLOMAP model was published by *Dunne et al.* [2016]. Based on these studies, we expect iodine oxides to be fairly well correlated to marine sulfur sources and amines to be well correlated to ammonia and H_2SO_4. Therefore, the effects of these compounds on our main results are likely to be smaller than the effects of uncertainties in the nucleation mechanisms we represent explicitly.

The chamber measurements of NPF of organic molecules with sulfuric acid, also part of the *Dunne et al.* [2016] model, are parametrized by *Riccobono et al.* [2014] as a function of sulfuric acid and 'BioOxOrg' molecular concentrations. The proxy 'BioOxOrg' is used to represent the large number of organic species that may contribute to the organic NPF. The BioOxOrg concentration was calculated as the reaction products of α-pinene with hydroxyl radicals. The constant $k_{SA\text{-}Org}$ in equation (3) for the NPF rate thus incorporates both the rate of the NPF process and, effectively, the fraction of the products of the α-pinene oxidation that are able to nucleate.

The chamber measurements of the NPF of organic molecules alone were performed later with improved instrumentation, which permitted us to measure directly the highly oxygenated organic molecules (HOMs) which may participate in NPF and the early growth of clusters. The fractions or "yields" of the oxidation products of α-pinene with OH and O_3 that result in HOMs are also measured at the CLOUD chamber [*Kirkby et al.*, 2016]. In our model, the molar yield of HOMs from the reaction of monoterpenes with O_3 is 1.4% and that with OH is 0.6%. Following *Tröstl et al.* [2016], these values are half the values measured in the CLOUD chamber because α-pinene produces more HOMs than the average monoterpene [*Jokinen et al.*, 2015]. Given this new knowledge, we also apply a single prefactor of 0.5 to the BioOxOrg-H_2SO_4 formation rate, as BioOxOrg

is itself a proxy for HOMs from α-pinene. There are large uncertainties in the yields associated with competing chemical mechanisms for terpene oxidation, the role of other important compounds such as isoprene, and the temperature dependence of the rates of the reactions in this treatment. These uncertainties are discussed further by *Gordon et al.* [2016].

NPF rates at 1.7 nm mobility equivalent diameter are thus calculated as the sum of the following parametrizations:

1. Binary neutral (indicated by *b*, *n*) and ion-induced (*b*, *i*) NPF involving sulfuric acid [*Dunne et al.*, 2016]:

$$J_{SA} = k_{b,n}(T)[H_2SO_4]^{p_{b,n}} + k_{b,i}(T)[H_2SO_4]^{p_{b,i}}[n_-] \quad (1)$$

   where the $k(T)$ are temperature-dependent prefactors (and include free-fitting parameters), p_i are constant free parameters, and $[n_-]$ is the concentration of negative ions in the chamber.
2. Ternary neutral (indicated by *t*, *n*) and ion-induced (*t*, *i*) NPF involving sulfuric acid and ammonia [*Dunne et al.*, 2016]:

$$J_{SA,NH3} = k_{t,n}(T)f_n([NH_3],[H_2SO_4])[H_2SO_4]^{p_{t,n}} + k_{t,i}(T)f_i([NH_3],[H_2SO_4])[H_2SO_4]^{p_{t,i}}[n_-] \quad (2)$$

   where the $f([NH_3],[H_2SO_4])$ are functions of the ammonia and sulfuric acid concentrations, also involving free-fitting parameters.
3. NPF of organics with sulfuric acid [*Riccobono et al.*, 2014]:

$$J_{SA\text{-}org} = 0.5k_{SA\text{-}Org}[H_2SO_4]^2[BioOxOrg] \quad (3)$$

   where BioOxOrg refers to the oxidation products of monoterpenes with OH, the fitted parameter $k_{SA\text{-}Org} = 3.27 \times 10^{-21}$ cm^6 s^{-1}, and, as described above, the factor 0.5 corrects for the large yield of HOMs from α-pinene compared to other terpenes found by *Jokinen et al.* [2015].
4. NPF from organics alone, a sum of neutral ($J_{n,org}$) and ion-induced ($J_{iin,org}$) components [*Kirkby et al.*, 2016]:

$$J_{org} = J_n + J_{iin} \quad (4)$$

$$J_n = a_1[HOM]^{a_2 + a_5/[HOM]} \quad (5)$$

$$J_{iin} = a_3[HOM]^{a_4 + a_5/[HOM]}[n_\pm] \quad (6)$$

   where HOMs are produced as described above but given here for convenience in units of 10^7 molecules cm^{-3}, $n_\pm$ is the ion concentration (equal to n_-, but ions of both sign participate in this NPF process), and a_i are free parameters. The information needed to reproduce the full parametrization given gas and ion concentrations is given in supporting information Text S1 and Table S1.

The organic NPF rates in our model are temperature independent, although *Yu et al.* [2016] suggest that introducing a temperature dependence calculated from quantum chemistry simulations has a strong effect on the organic NPF rates. *Yu et al.* [2016] highlight an important uncertainty, but we note that the production rate of the low volatility organic molecules that participate in NPF is also temperature dependent [*Crounse et al.*, 2013]. These molecules are thought to be primarily produced by an autoxidation reaction [*Ehn et al.*, 2014]. This reaction accelerates at high temperature and competes more effectively with the termination reactions that remove peroxy radicals and stop the formation of HOMs. Therefore, decreases in NPF rate at high temperature are offset, to a currently unknown extent, by an increased yield of molecules able to nucleate. In view of this uncertainty we do not include any temperature dependence for the organic NPF rates. A remaining temperature dependence would mainly affect the altitude dependence of organic nucleation and the relative fractions of inorganic and organic nucleation above the boundary layer.

Our formation rates are adjusted to account for losses during the initial growth (to 3 nm, whereupon they enter the nucleation mode) with the equation of *Kerminen and Kulmala* [2002]:

$$J_3 = J_{1.7}\exp\left(-0.23\frac{CS}{GR}\left(\frac{1}{1.7} - \frac{1}{3}\right)\right) \quad (7)$$

where *CS* is the condensation sink in s^{-1} and *GR* is the growth rate in nm h^{-1}, equal to

$$GR = 7.3 \times 10^{-8}[H_2SO_4] + 1.41 \times 10^{-7}[HOM] \quad (8)$$

where the term involving [HOM] is an approximate form of the parametrization of *Tröstl et al.* [2016] and the term involving [H_2SO_4] is based on the study by *Nieminen et al.* [2010]. We assume that the oxidation conditions in the CLOUD chamber represent those in the atmosphere accurately enough to produce representative HOMs and NPF rates. There is evidence that this assumption is valid in comparisons of the mass spectra to atmospheric data in a study by *Schobesberger et al.* [2013]. It is discussed further by *Gordon et al.* [2016].

We do not comprehensively reevaluate our model as, apart from the different representation of the aerosol size distribution, it is very similar to that used by *Dunne et al.* [2016]. We compare modeled and observed CCN in supporting information Text S2 and investigate how the modal aerosol size distribution affects the results compared to the sectional structure used by *Dunne et al.* [2016] in supporting information Text S3.

Present-day simulations are run for 2008, and preindustrial simulations are run with 2008 meteorology (for direct comparison of the aerosol with the present-day run) and emissions designed to represent the year 1750. For this 1750 simulation, anthropogenic sources of SO_2 and H_2SO_4 are removed from the model, OH, NO_3, and ozone concentrations are adjusted to preindustrial levels as described above, and black and organic carbon primary emissions are adjusted to a representation of preindustrial levels at the year 1750 [*Dentener et al.*, 2006]. Ammonia emissions due to fossil fuel use, biofuel combustion, industry, synthetic fertilizers, crops, domestic animals, and humans are also removed, leaving only emissions from wild animals, soils under natural vegetation, and oceans [*Dunne et al.*, 2016]. The concentration of VOCs is not changed: VOCs are assumed to be biogenic, not anthropogenic, and changes in vegetation type are not considered. Land use changes are also likely to affect many model processes, especially BVOC, fire and ammonia emissions, but the scale and sometimes even the sign of the effects are not known with confidence [*Heald and Spracklen*, 2015], so we do not represent land use changes in our preindustrial simulations.

3. Methods

The importance of NPF is quantified by the fractions of the total concentration of particles greater than 3 nm in diameter (N_3) and of CCN that originate from NPF. In Figures 1–4 and throughout the text, we approximate these fractions as $1 - n_{prim}/n_{tot}$. In this equation, n_{tot} is the annual mean number concentration of particles over the specified model levels in a simulation with NPF and primary emissions, and n_{prim} is the concentrations of particles in a simulation with primary emissions but without NPF. In this way we approximate the fraction of CCN that originate from new particle formation as the relative change to CCN concentrations when new particle formation is included in the model.

The contribution of NPF is determined by removing it from the model rather than by removing primary particles because removing NPF has (to first order) no effect on primary CCN, while removing primary emissions leads to a substantial reduction in the condensation sink. This reduction of the sink then causes NPF rates to increase, leading to an increase of around 35% in total ground-level particle numbers in both present-day and preindustrial conditions. Removing NPF also reduces the condensation sink, but the reduction is much smaller, because nucleated particles generally have much smaller surface areas than primary particles. Furthermore, any reduction in the condensation sink has a much smaller effect on CCN formation by primary particles than on CCN formation by nucleated particles, because primary particles are usually emitted with larger diameters, so grow more quickly by condensation to CCN size. The same attribution technique was also used, and discussed further, by *Merikanto et al.* [2009].

In our model, NPF is simulated as occurring homogeneously across each model grid box. Close to, or inside, sources such as power plant smoke stacks or vehicle exhausts, NPF will occur at much higher rates than our model can capture. New particles from these highly localized sources are modeled as primary emissions of sulfate or carbonaceous particles, with a lognormal size distribution prescribed by *Stier et al.* [2005]. We consider all of these emissions to be primary, following *Merikanto et al.* [2009], and do not remove them when we remove NPF from our model. This has a small but nonnegligible effect on our main results (see section 4). Primary sulfate emissions were studied in the GEOS-chem model by *Luo and Yu* [2011], who found modeled particle concentrations were sensitive to the size distribution of the emitted sulfate.

4. Importance of New Particle Formation in CCN Formation

Annually averaged at low cloud level, 54% of CCN concentrations at 0.2% supersaturation (CCN0.2%) originate from NPF in the present-day atmosphere (with an estimated uncertainty range of 38–66%, obtained

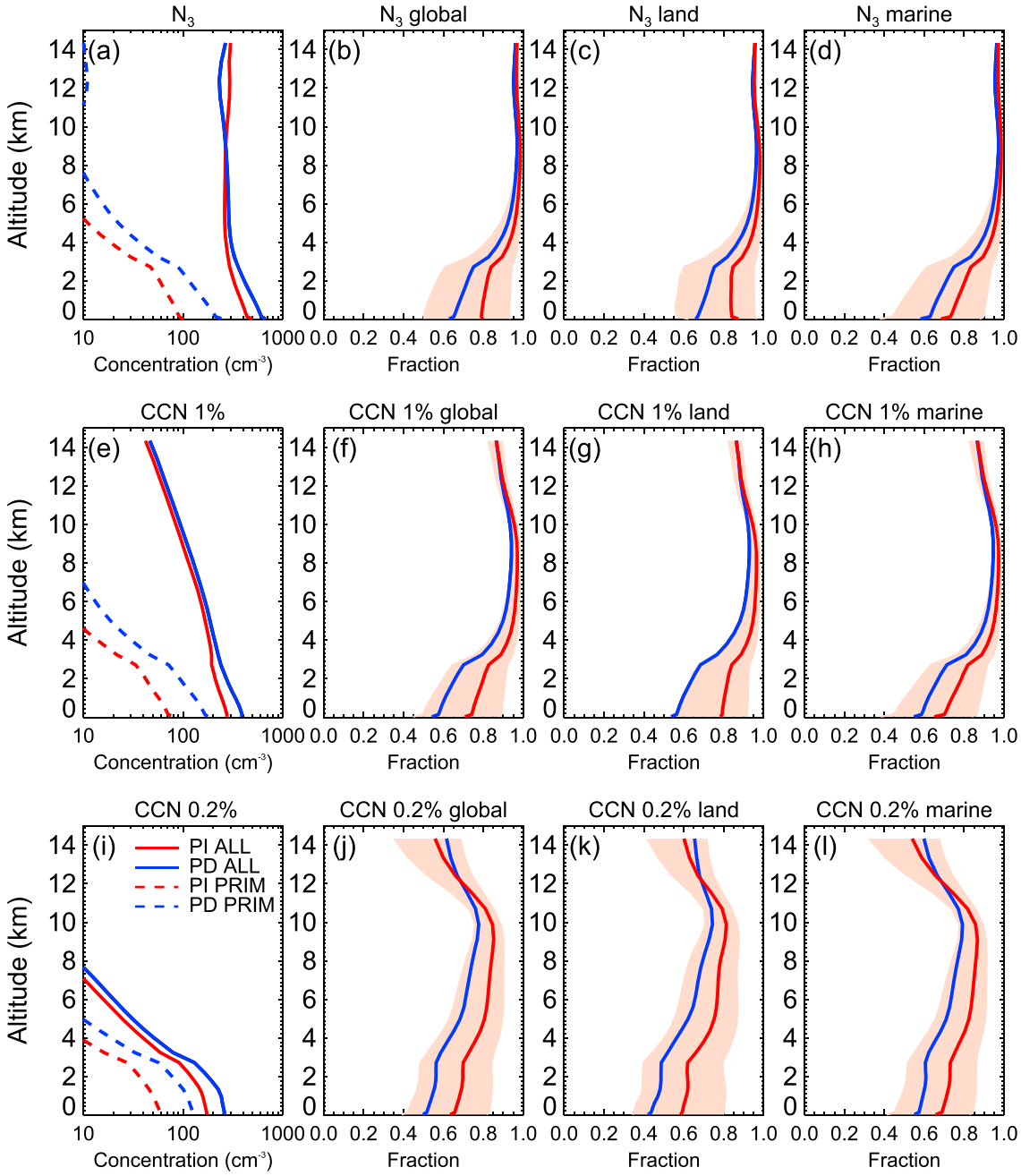

Figure 1. Particle concentrations and the fraction caused by NPF, (a–d) for N_3, (e–h) CCN at 1%, and (i–l) 0.2% supersaturations. The altitude dependence of annual global mean preindustrial (red) and present-day (blue) particle concentrations is shown in Figures 1a, 1e, and 1i and the fraction of these particles originating from NPF in Figures 1b–1d, 1f–1h, and 1j–1l. All concentrations are calculated at ambient temperature and pressure. Figures 1a, 1e, and 1i also show the concentration of primary particles in present-day conditions (blue dashed) and preindustrial conditions (red dashed). In Figures 1b–1d, 1f–1h, and 1j–1l, the fraction of CCN that originate from NPF is shown in red for preindustrial and blue for present-day, and the estimated uncertainty is given by the shaded region, for preindustrial only. The present-day uncertainty is correlated to the preindustrial. These subparts show that higher fractions of CCN originate from NPF at high altitude and in marine regions.

as described in section 6). We define low cloud level in our model as the average over the two model levels between approximately 460 and 1100 m altitude. In the preindustrial atmosphere, 67% of CCN0.2% at low cloud level originate from NPF, with an uncertainty range of 45–84%. Fuller results are given in Table 1 and show that at all altitudes, a higher fraction of all particles greater than 3 nm in diameter originate from NPF than do CCN, as expected. It seems probable that, especially before the Industrial Revolution, NPF was responsible for more than half of climate-relevant particles.

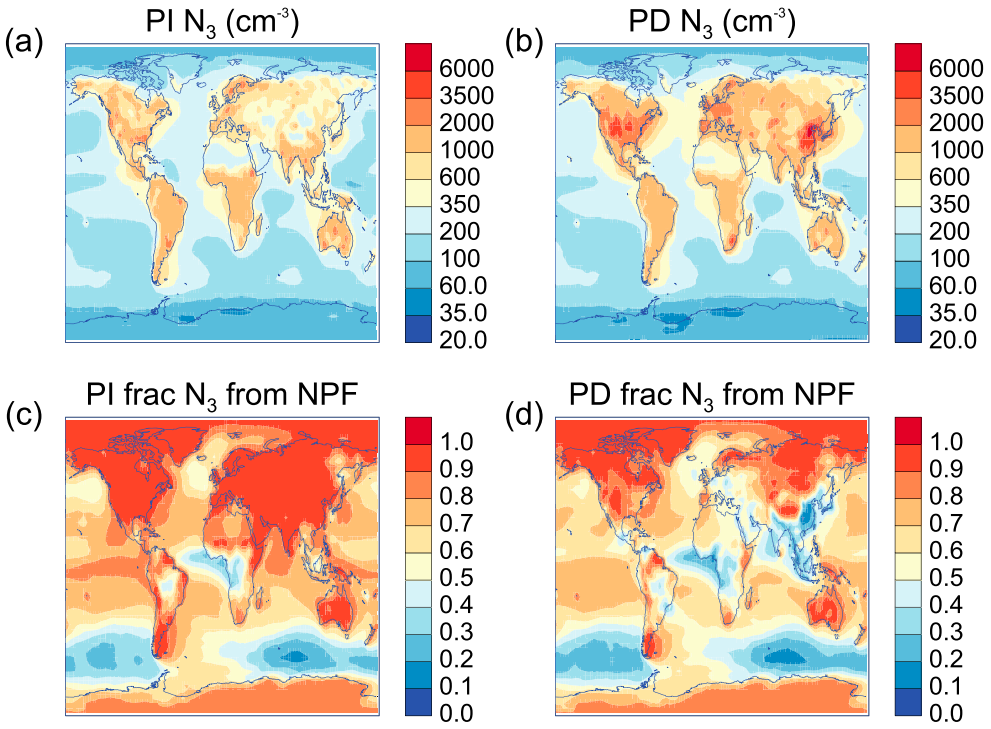

Figure 2. Particle number concentrations (N_3) within approximately 460 m of the surface and fractions of N_3 from NPF. (a) The present-day and (b) preindustrial annual mean concentrations of all particles greater than 3 nm in diameter; (c, d) the fractions of these particles that originate from NPF. These fractions are approximated by the relative change in particle concentrations when NPF is switched off in the model. The altitude range is below the level of most clouds.

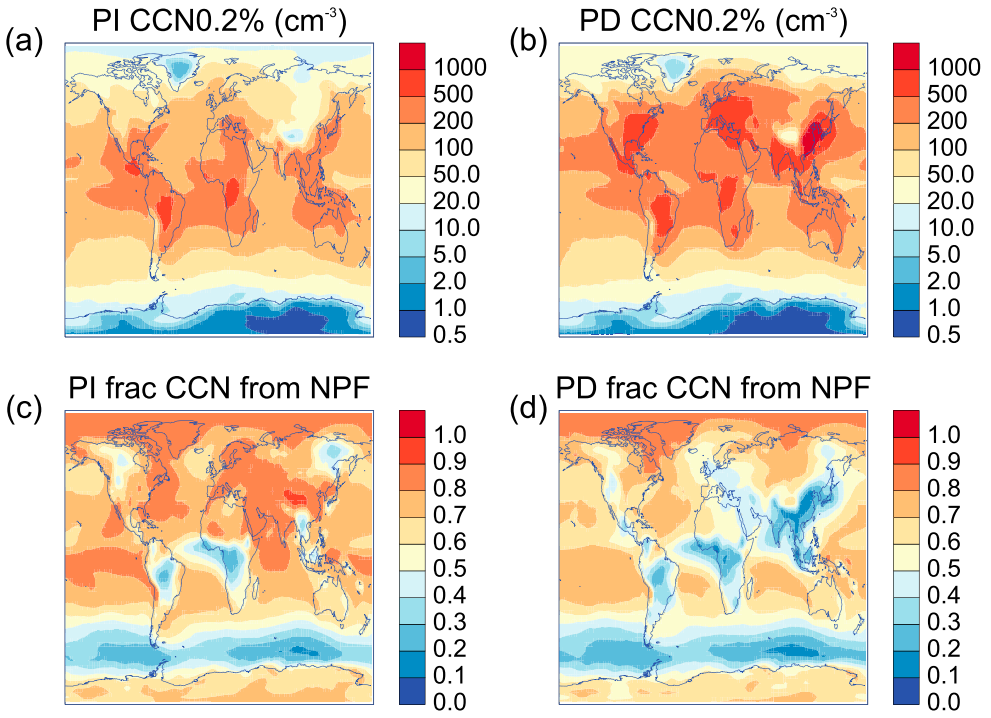

Figure 3. CCN concentrations at 0.2% supersaturation (CCN0.2%) at low cloud level (approximately 460–1100 m altitude), and fractions from NPF. The (a) present-day and (b) preindustrial annual mean concentrations; and (c, d) the fractions of these particles that originate from NPF.

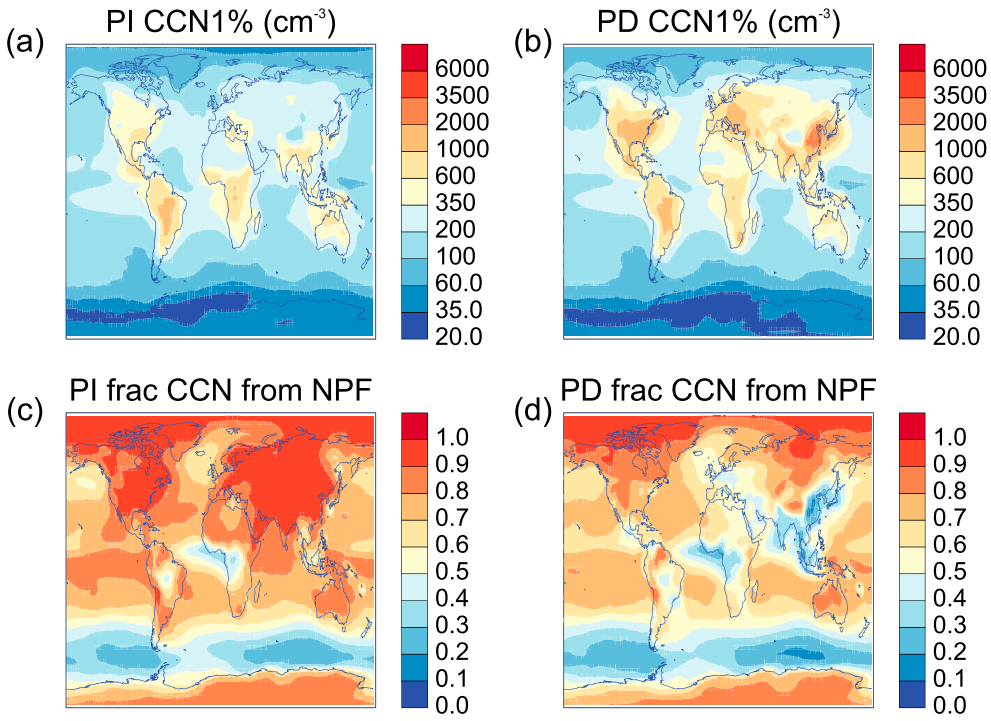

Figure 4. CCN concentrations at 1.0% supersaturation at low cloud level (approximately 460–1100 m altitude), and fractions from NPF. The (a) present-day and (b) preindustrial annual mean concentrations; (c, d) the fractions of these particles that originate from NPF.

There is a strong seasonal dependence in both hemispheres, with more CCN0.2% resulting from NPF in local summers than in winters (for example, 79% in July compared to 56% in January, at low cloud level in the preindustrial Northern Hemisphere). This seasonal difference is likely due to the increased emissions of precursor vapors for NPF, particularly terpenes in the summer months due to warmer temperatures, and the increased concentration of the hydroxyl radicals needed to oxidize sulfur dioxide and organic molecules.

At 1.0% supersaturation, smaller particles will activate, so on average, the contribution of NPF is greater than at 0.2%. At low cloud level in today's atmosphere, 60% of CCN at 1% supersaturation (CCN1%) originate from NPF (range 44–73%). In the preindustrial atmosphere the fraction is 76% (range 52–89%). In some of the cleaner parts of the preindustrial atmosphere, the average supersaturation at which CCN activated may have been (slightly) higher than it is today, because there were fewer CCN overall. While NPF is more important in determining the concentration of smaller particles, we note that the spatial dependence (discussed later) suggests that convective systems in which supersaturations are high enough to activate these particles are not necessarily colocated with areas in which these CCN are dominated by NPF.

Figure 1 shows that above both land and ocean, more CCN result from NPF in the pre-industrial atmosphere than in the present-day atmosphere. This change is mainly due to the large increase in primary emissions from the continents over the industrial period, and these primary emissions are readily advected over the oceans. As noted by *Merikanto et al.* [2009], the fraction of CCN from NPF increases with altitude and is higher in marine regions than over land. Figures 1a, 1e, and 1i demonstrate that the total particle number is roughly independent of altitude, while the primary particles decrease further from the surface source. The total concentration of particles that can act as CCN at low supersaturations also decreases rapidly above 3 km, but where 1% supersaturations occur there are similar numbers of CCN at all altitudes.

Figures 2–4 show that the importance of NPF varies widely across the globe. The fraction of CCN0.2% from NPF in Figure 3 never gets close to 100%, but it is usually greater than 50%, except in regions of high sea spray, biomass burning, or high human population density. The fraction never approaches 100% because there is always some transport of primary particles, and while the numbers of these are low compared to N_3 in Figure 2, they do contribute significantly to CCN. Surface particle numbers over land in the preindustrial Northern Hemisphere (Figure 2a) are almost entirely due to NPF, while in the Southern Ocean,

Table 1. Percentages of Particle Number That Originate From NPF in Present-Day and Preindustrial Atmospheres[a]

	Percent of Particles From NPF				
	January NH (Winter)	July NH (Summer)	January SH (Summer)	July SH (Winter)	Overall -
			Present Day		
Surface N_3	64.2	72.5	74.7	52.7	65.4
Surface CCN 0.2%	43.4	57.2	58.1	43.3	51.8
Cloud level N_3	71.0	75.3	78.6	53.5	67.7
Cloud level CCN 1%	53.4	68.9	70.6	50.7	60.0
Cloud level CCN 0.2%	45.8	59.7	62.0	46.2	53.8
FT and UT N_3	81.1	90.0	86.7	87.3	90.6
			Preindustrial		
Surface N_3	74.3	91.8	79.7	58.2	79.3
Surface CCN 0.2%	52.7	77.3	64.6	49.6	65.5
Cloud level N_3	74.5	92.2	83.6	58.4	79.8
Cloud level CCN 1%	63.1	89.3	77.0	58.2	75.9
Cloud level CCN 0.2%	55.7	78.9	68.9	52.4	67.4
FT and UT N_3	78.6	95.4	88.1	88.5	93.3

[a]The first four columns give an indication of the seasonal cycle in the Northern Hemisphere and Southern Hemisphere, while the last column gives the annual mean at the altitude level specified, where "Surface" denotes the mean from the surface to around 460 m altitude; "cloud level" the level of low clouds, from around 460 to 1100 m altitude; and "FT and UT" means "free and upper troposphere," defined by altitudes from 1.5 km to the top of the troposphere. The particle numbers are calculated at ambient temperature and pressure.

CCN and particle number concentrations are both dominated by primary sea spray (Figure 2c). Most CCN are also primary in West Africa, the Amazon, and Canada, due to biomass burning (Figures 3c and 3d, and 4c and 4d). The key differences in the preindustrial atmosphere compared to the present day are due to the lack of polluted regions with very high primary emissions and condensation sinks that suppress NPF in the Northern Hemisphere (compare Figures 3c and 3d). Before industrialization, almost all N_3 over Asia and North America originated from NPF, while today primary emissions are much more important (compare Figures 2c and 2d).

The spatial variations in particles produced by NPF are broadly consistent between models: for example, Figure 3b can be compared (approximately) to S1c of *Yu and Luo* [2009]. Our Figures 3d and S1d of *Yu and Luo* [2009] both pick out the key regions where primary emissions are expected to dominate, but the *Yu and Luo* [2009] study suggests that NPF is more important over oceans than our study, probably due to the increased importance of sulfuric acid in the NPF mechanism [*Yu and Luo*, 2009, Figure 6e].

CCN1%, shown in Figure 4, are especially important in regions of high convection, and show similar spatial patterns to N_3 concentrations. As expected from the global average, NPF contributes more to these particles than to CCN0.2%, and this is particularly clear in preindustrial Asia (Figure 4c), where primary preindustrial emissions are insignificant compared to NPF as a source of particles at this size in our model. Regions in which CCN at 1% supersaturation are dominated by NPF coincide with tropical convection where 1% supersaturations are likely to occur in southern China, but not in Mongolia or Russia. The African convective systems are dominated by primary emissions.

If we consider subgrid sulfate emissions to be NPF and remove them from the model as well as removing explicitly parameterized NPF, we find a slightly larger change to CCN concentrations: we would estimate that 58% of cloud-level CCN0.2% originate from NPF in the present-day atmosphere and 71% in the preindustrial. Full results are given in supporting information Table S12.

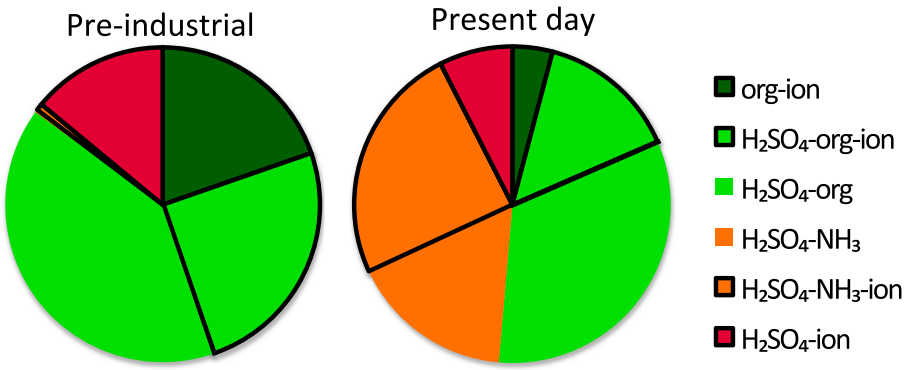

Figure 5. Fractions of NPF from organic ("org-ion," "H_2SO_4-org," and "H_2SO_4-org-ion" (green)) and inorganic ("H_2SO_4-ion" (dark red), "H_2SO_4-NH_3" (orange), and "H_2SO_4-NH_3-ion" (orange)) pathways in preindustrial and present-day atmospheres, annually averaged within 5.8 km of the surface. Biogenic vapors are abbreviated to "org." Neutral and ion-induced NPF fractions are separated, in accordance with the results in section 8. The ion-induced fraction of ternary organic (H_2SO_4-org-ion) NPF is included, but it is not as well constrained by available CLOUD measurements as the overall fraction of ternary organic NPF (see section 8). Neutral NPF of pure sulfuric acid and pure biogenic vapors are responsible for less than 0.5% of particle formation at these altitudes, so these pathways are not shown. The numerical values of the fractions are given in supporting information Table S2.

5. Comparison of Results to Previous Work With the Same Model

We estimate that 54% of CCN0.2% (range 38–66%) originate from NPF in the present-day atmosphere, while *Merikanto et al.* [2009] estimate that 45% (31–49%) originate from NPF; we thus conclude that NPF probably exceeds primary emissions as a source of CCN. However, while *Merikanto et al.* [2009] estimated that 75% of all particles (N_3) at the surface originated from NPF, our estimate is lower, at 65% (range 42–77%). In contrast to the uncertainty range for the CCN estimate, this uncertainty range is smaller than that of *Merikanto et al.* [2009] and fits inside the 37–84% range they quote.

Much of the difference compared to *Merikanto et al.* [2009] is likely due to the different treatment of the aerosol size distribution explained in supporting information Text S3. *Dunne et al.* [2016] calculate that 42.7% of CCN originate from NPF in the present-day atmosphere, with a very similar NPF scheme to that of the current study (pure biogenic NPF is not included, but its effect in the present-day atmosphere is small). An investigation of this discrepancy is presented in supporting information Text S3.

Marine surface total particle number concentrations in our simulations (Figure 2) are strikingly lower than those of *Merikanto et al.* [2009] Figure 5. The difference is because the boundary layer NPF mechanism of *Merikanto et al.* [2009] involved the activation of clusters by sulfuric acid molecules [*Kulmala et al.*, 2006]. In that model, relatively low sulfuric acid concentrations were sufficient to produce high boundary layer NPF rates, and such sulfuric acid concentrations exist over (for example) the Southern Ocean. In our updated model, high ammonia or organic concentrations are also required for NPF, except in the upper troposphere where the temperature is low enough for binary NPF of sulfuric acid to be important [*Dunne et al.*, 2016], and the concentrations of ammonia and organics are not high enough over the Southern Ocean for NPF to proceed at such high rates.

6. Model Uncertainties

Here we assume that the uncertainty in the fraction of CCN from NPF depends only on two factors: the uncertainty in emissions of primary particles and the uncertainty in emissions of the precursor vapors for NPF and particle growth by condensation. These components have simple, well-defined effects on either the primary or the secondary particles: for example, increased vapor emissions will increase the fraction of CCN from NPF, while increased primary particle emissions will decrease it. We use the expert elicitations of *Lee et al.* [2013] and *Carslaw et al.* [2013] to guide our estimates of these uncertainties.

We do not study separately the uncertainty in processes whose rates are highly correlated with vapor emissions or concentrations. For example, there is an uncertainty in the growth rate of newly formed aerosols due to the use of proxy organic compounds to represent the complex mixture in the real atmosphere

Table 2. Summary of Parameter Perturbations Used to Determine the Uncertainty in the Fractions of Particle Number Concentrations That Originate From NPF[a]

Parameter	Description	Baseline	Low Emission	High Emission
BB_EMS	BC/OC biomass burning emission rate scale factor	1	0.5	2
BB_DIAM	BC/OC emitted mode diameter (biomass burning)	150 nm	175 nm	125 nm
SS_ACC	Sea spray mass flux (scale factor)	1	0.4	2.5
ANTH_SO2	Anthropogenic SO_2 emission flux scale factor	1	0.8	1.25
VOLC_SO2	Volcanic SO_2 emission flux scale factor	1	0.67	1.5
DMS_FLUX	DMS emission flux scale factor	1	0.67	1.5
BIO_SOA	Biogenic monoterpene production of SOA	1	0.25	4

[a]The model is run with either all low or all high primary particle emissions and baseline vapor concentrations (second to fourth rows) and then again with baseline primary particle emissions and either all low or all high vapor emissions (fifth to eighth rows). The production of secondary organic aerosol from biogenic monoterpenes is varied by applying the scale factor to the terpene emissions directly.

[*Tröstl et al.*, 2016]. The model also does not simulate the dependence of growth rates on particle diameter due to the Kelvin effect for particles with diameters above 3 nm. However, to a good approximation, the growth rates vary linearly with the relevant vapor concentrations. Therefore, provided the perturbations to the vapor emissions parameters are sufficiently large, they can account for the uncertainties in the growth rates without separate studies. Necessarily, however, some uncertainties are not accounted for. For example, we do not include anthropogenic secondary organic aerosol (SOA) in our model nor do we fully treat the effects of SOA volatility. These omissions must lead to model biases over land, but the agreement of the model with particle concentrations measured at land surface stations [*Dunne et al.*, 2016] suggests the biases are small.

To determine our uncertainties, we construct perturbed versions of the model with high and low primary emissions, and versions with high and low vapor emissions. Assuming the uncertainties in our selected vapor and particulate emissions are uncorrelated, we add the differences between the fractions of CCN resulting from NPF from these model runs and the baseline runs in quadrature to determine the overall uncertainty ranges. Thus, the overall uncertainty σ is

$$\sigma = \sqrt{\sum_i \sigma_i^2} \tag{9}$$

where the σ_i are determined from the differences in global annual mean fractions of concentrations that originate from NPF between the baseline and perturbed model runs. The perturbations are summarized in Table 2. The parameters are selected to try to represent the major components of the uncertainty reasonably well over the whole planet, hence the inclusion of the sea spray mass flux, which is relatively unimportant on average but dominates the uncertainty in extensive marine regions. Furthermore, an attempt is made to prioritize variation of parameters that are likely to dominate the uncertainty in preindustrial CCN concentrations, hence the inclusion of volcanic SO_2 and DMS, and the choice to vary biogenic rather than anthropogenic secondary organic emissions (in fact, anthropogenic secondary organic emissions are not included in the model version we use here). In *Lee et al.* [2013], ranges are defined by expert elicitation such that the parameter is "highly unlikely" to lie outside the range. Here we assume this means the ranges represent approximately 2 sigma uncertainties, and we choose perturbations here to be roughly half the size of those of *Lee et al.* [2013]. While this uncertainty estimation is clearly somewhat subjective, the use of the perturbed parameter ensembles from previous work allows the important variables to be prioritized. The uncertainty ranges we obtain from the perturbed model runs are summarized in Table 3.

Additional checks, e.g., varying the Aitken mode width or our simulated preindustrial ammonia concentrations, led to smaller perturbations to the fractions of CCN from NPF, of at most around 3% (see supporting information tables). Since pure organic NPF rates are currently very uncertain, we checked the sensitivity of our results to these uncertainties by simply removing pure biogenic NPF from the model. We find that even in the pre-industrial atmosphere, the sensitivity to pure biogenic NPF is within our uncertainty range: the fraction of low-cloud-level CCN originating from NPF decreases from 68% to 63% when it is removed. Despite the fact that over half of new particles in the first 500 m altitude in this model are produced via the pure biogenic pathway and it is important in certain regions [*Gordon et al.*, 2016], it is relatively unimportant at higher

Table 3. Importance of New Particle Formation in Simulations With Perturbed Emissions[a]

	Baseline (%)	Low to High Vapors (%)	High to Low Primaries (%)
Present-day N_3	65	55–73	48–75
Preindustrial N_3	79	67–86	53–92
Present-day CCN 0.2%	54	47–62	40–63
Preindustrial CCN 0.2%	67	61–75	46–82
Present-day CCN 1%	60	52–69	46–69
Preindustrial CCN 1%	76	68–83	54–88

[a]The annual mean percentage of all particles greater than 3 nm in diameter within around 460 m of the surface (second and third rows) and low cloud level CCN at 1% and 0.2% (fourth to seventh rows) that originate from new particle formation (NPF) in the preindustrial and present-day atmospheres, in the baseline, low-emission, and high-emission scenarios. These values are used to determine the uncertainty ranges for the fractions of CCN that originate from NPF.

altitudes compared to the new inorganic NPF mechanism of *Dunne et al.* [2016], and when it is removed from the model, other NPF mechanisms take over. The insensitivity of our global averages to pure biogenic NPF also suggests that uncertainties in the other NPF parametrizations, for example, the omission of a dependence on relative humidity (the effect of which was studied by *Dunne et al.* [2016]), will not lead to large effects on globally averaged CCN concentrations. This supports previous studies by, for example, *Westervelt et al.* [2014] and *Spracklen et al.* [2008], who found that CCN concentrations were relatively insensitive to perturbations to NPF rates.

7. Relative Importance of Organic and Inorganic New Particle Formation Pathways

In our model, 51% of present-day NPF below 5.8 km altitude involves organic molecules and 49% does not. Almost all NPF involves sulfuric acid. The contribution of the various NPF pathways is calculated by comparing the annual average formation rates of 3 nm particles in the model below 5.8 km altitude. The fractions are shown in Figure 5 and enumerated in supporting information Table S2. We quote fractions below 5.8 km (the top of the fourteenth model level from the surface) because we assume most activation of CCN takes place at these altitudes. In the preindustrial atmosphere, 86% of NPF involves organic molecules and 14% does not. Of the total, 20% is pure organic in the preindustrial atmosphere and 4.1% in the present day. Figure 5 also shows that binary ion-induced NPF of sulfuric acid and water was more important in the preindustrial atmosphere than it is today. This is because ammonia concentrations were lower in the preindustrial atmosphere. Between 5.8 km altitude and the top of the troposphere, over 85% of NPF is entirely inorganic in both preindustrial and present day. In the present-day atmosphere, 77% of NPF at these altitudes involves only sulfuric acid and water, 16% involves ammonia and 7.2% organics. In the preindustrial, 88% of NPF at these altitudes involves only sulfuric acid and water, 0.1% involves ammonia, and 12% organics.

We note that all of these fractions are still very uncertain. Rather than attempting to quantify the uncertainties here, we refer the reader to the extensive discussion and sensitivity studies in the supporting information of *Dunne et al.* [2016], and for pure biogenic NPF to *Gordon et al.* [2016]. Paraphrasing these publications, the uncertainties in organic NPF are greater than those in the pure inorganic pathways and are driven by the unknown temperature dependence [*Yu et al.*, 2016], the lack of complete chemical mechanisms, and limited knowledge of the atmospheric lifetime of the organic species that nucleate. The uncertainty in the pure inorganic pathway is probably dominated by uncertain knowledge of atmospheric ammonia and sulfuric acid concentrations. Additional uncertainties stem from the omission of anthropogenic organic compounds and amines from the system.

8. Importance of Cosmic Ray Ions for New Particle Formation and CCN

Ions from cosmic rays and radon gas participate in both inorganic and organic NPF. Within 5.8 km of the surface, where we assume most activation of CCN takes place, 50% of NPF in the present-day atmosphere and 59% in the preindustrial atmosphere involve ions. The calculations are summarized in Figure 5. We assume that between 0% and 60% of the organic-H_2SO_4 NPF rate is ion induced, depending on the NPF rate [*Dunne et al.*, 2016], from an approximate fit to Figure 1D of *Riccobono et al.* [2014]. However, the ion-induced fraction of NPF involving organics and sulfuric acid together is poorly known at present. Figure 5 shows that in the present-day atmosphere, nearly half of the ion-induced NPF (and 29% of the total NPF rate) is inorganic ternary ion-induced NPF of ammonia, sulfuric acid, and water. In the preindustrial atmosphere, however, less than 0.1% of the total NPF rate is ternary inorganic ion-induced NPF. Instead, most NPF is ternary organic neutral

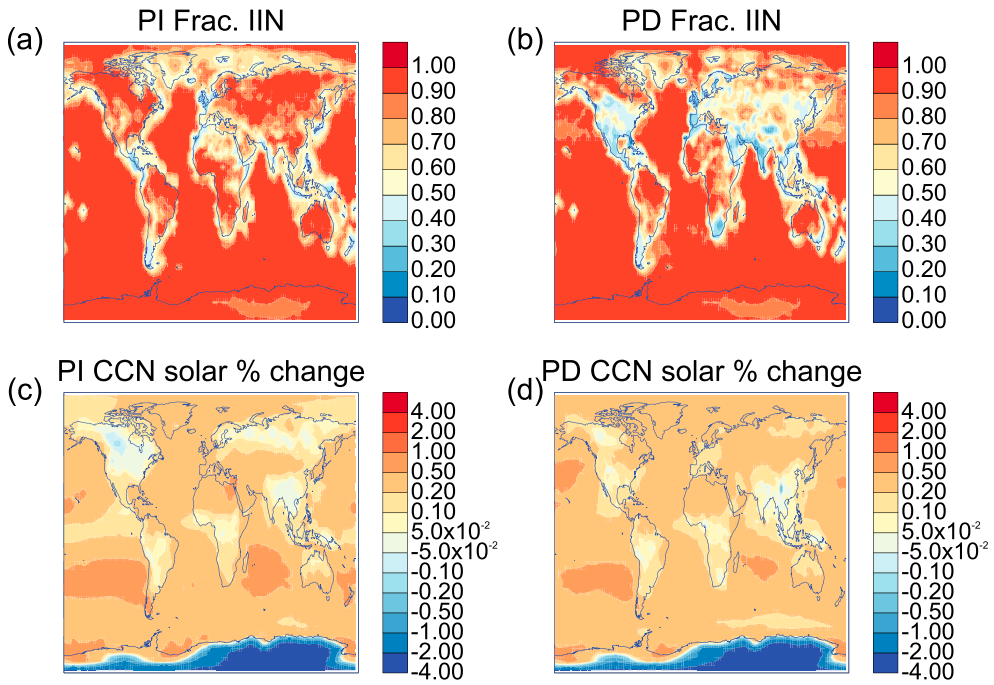

Figure 6. Annually averaged fractions of ion-induced new particle formation between the surface at 5.8 km altitude, and percentage changes to low-cloud-level CCN between solar maximum and solar minimum. (a, c) Preindustrial and (b, d) present-day conditions are shown in each case. Figures 6a and 6b show that the fraction of ion-induced NPF tends to be high where the overall NPF rate is low; therefore, the fraction of new particles produced via ion-induced NPF is lower than the figure suggests.

and ion-induced NPF, pure organic ion-induced NPF, and inorganic binary ion-induced NPF (supporting information Table S2). However, the uncertainty in the preindustrial estimate of ammonia concentrations is large [*Dunne et al.*, 2016].

The spatial variation of the relative contribution of ion-induced NPF, averaged over altitudes within approximately 5.8 km of the surface, is shown in Figure 6. Usually ion-induced NPF dominates whenever overall NPF rates are relatively low, especially over oceans. In our model, NPF is more likely to be neutral along coastlines, where marine sulfuric acid and organics from land can mix and therefore ions are not as important to stabilize clusters. At low altitudes, ion-induced NPF should be particularly dominant today in tropical land regions and the remote boreal forests of northern Canada and Siberia.

In our simulations, setting the ion concentration to zero results in 11% fewer CCN0.2% in the present-day atmosphere. This is similar to the change of 9.3% found by *Yu et al.* [2012], who used a model for ion-induced binary NPF of sulfuric acid. In the preindustrial atmosphere, the corresponding change we find is 20%. These changes are, however, not estimates of the fraction of CCN that result from ion-induced NPF, which is much higher than these numbers suggest. These changes to CCN include a strong negative feedback: if no ions participate in NPF, the condensation sink falls, allowing the neutral NPF rates to rise, and the change in CCN is small.

To estimate the proportion of CCN that result from ion-induced NPF, we multiply the fractions of NPF that are ion-induced within 5.8 km of the surface by the fraction of low-cloud-level CCN that originate from NPF. This is, as always, approximated by the change in CCN when new particle formation is switched on in our model. We find that 27% of low-cloud-level CCN originate from ion-induced NPF in the present-day atmosphere and 40% in the preindustrial. The larger altitude range used for the fraction of ion-induced NPF fraction compared to the fraction of CCN from NPF reflects the substantial mixing that occurs during the growth of particles to CCN size. The dependence on the range of altitudes chosen for each fraction is relatively weak: if all particles below 10 km altitude contribute to CCN formation at low cloud level, the present-day fraction increases to 30% and the preindustrial fraction increases to 47%.

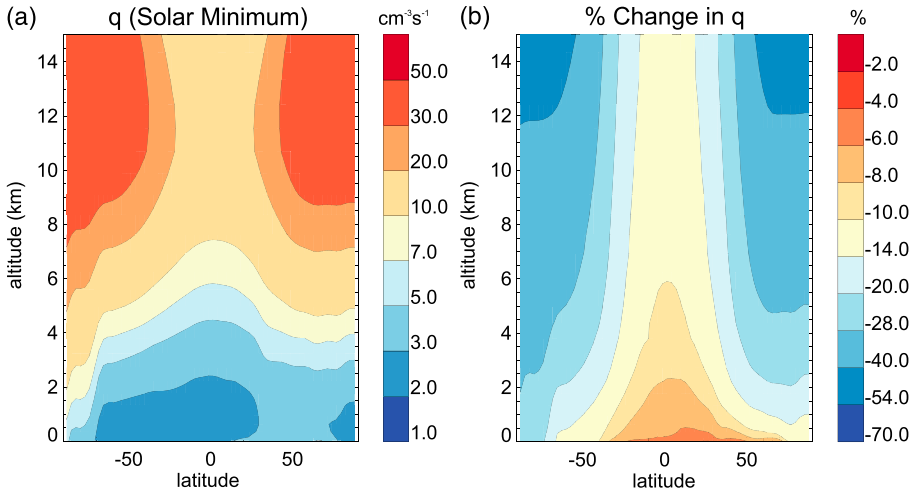

Figure 7. (a) Zonally and annually averaged overall ion production rates (due to cosmic rays and radon) in GLOMAP and (b) the percentage change in ion production rate over the 22 year solar cycle. An identical figure appears in the supporting information of *Dunne et al.* [2016].

To determine the effect of variations in the cosmic ray intensity on CCN, we perturb the heliospheric modulation potential from its 2008 (solar minimum) level by a factor 3.56. This produces a potential similar to recent solar maxima, e.g., in 1991, so is representative of the 22 year solar cycle. The modulation potential representative of a solar maximum was applied to both preindustrial and present-day simulations. The 22 year cycle is predicted by *Usoskin et al.* [2015] to lead to a stronger effect on ionization rates than the Maunder Minimum between 1645 and 1700. The overall ion production rate due to radon and cosmic rays, and the effect of this change, is shown in Figure 7. By default our perturbation does not affect NPF of organic molecules with sulfuric acid, because of the way this NPF pathway is parametrized, but we test the effect of this assumption at the end of this section.

We find that realistic perturbations to ion concentrations only lead to small changes to present-day CCN concentrations, in accordance with the results of *Pierce and Adams* [2009b], *Snow-Kropla et al.* [2011], *Yu et al.* [2012], *Dunne et al.* [2012], *Kazil et al.* [2012], and *Yu and Luo* [2014a]. Further to these studies, we also find no significant effect in the preindustrial atmosphere. At most, the variation in cosmic ray ion production rate (vertical profiles shown in Figure 7) leads to a perturbation to low cloud level CCN0.2% of around 2%, as shown in Figure 6. The global annual mean change in low-cloud-level CCN0.2% is 0.3% in preindustrial and 0.2% in present-day conditions (Table 4). Slightly larger perturbations to the total particle number (N_3) concentrations are visible both at the surface (Figures 8a and 8b), where ion-induced pure biogenic NPF dominates the preindustrial NPF rate, and at high altitude (Figures 8c and 8d) where the solar cycle has a larger effect.

Table 4. The Effect of the Solar Cycle on Particle Number Concentrations[a]

	Percentage Change Over Solar Cycle				
	January NH (Winter)	July NH (Summer)	January SH (Summer)	July SH (Winter)	Overall
PI cloud CCN0.2%	0.2	0.3	0.4	0.2	0.3
PI surface N_3	0.4	0.8	0.8	0.4	0.6
PI FT and UT N_3	0.3	0.5	0.7	0.6	0.6
PD cloud CCN0.2%	0.2	0.2	0.3	0.2	0.2
PD surface N_3	0.6	0.4	0.6	0.3	0.4
PD FT and UT N_3	0.4	0.4	0.5	0.3	0.5

[a]Percentage changes to particle concentrations over the solar cycle are given for low-cloud-level CCN0.2%, N3 within 500 m of the surface, and N3 in the free and upper troposphere (FT and UT) in preindustrial (PI) and present-day (PD) simulations. The seasonal cycle is given by calculating changes for January and July in each hemisphere.

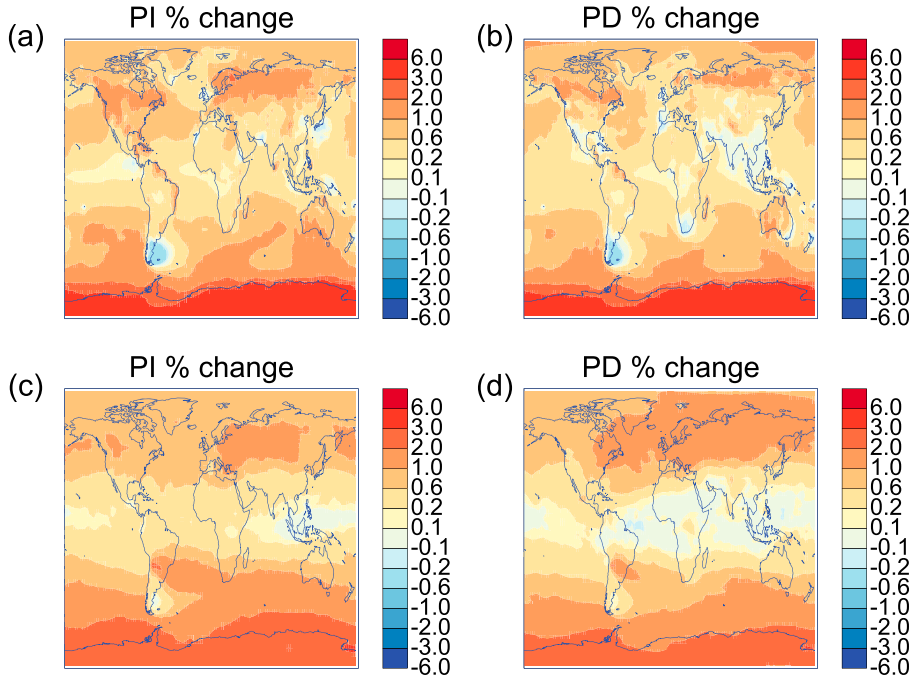

Figure 8. Annually averaged percentage changes to total particle number (N_3) concentrations (cm^{-3}) between solar maximum and solar minimum, within around 460 m of the surface in (a) preindustrial and (b) present-day conditions and at high altitude (between 1.5 km and the top of the troposphere), also in (c) preindustrial and (d) present-day conditions.

However, the annual average changes in these cases over the solar cycle are only 0.4–0.5% in the present day, and 0.6% in the preindustrial. Table 4 shows a slight seasonal cycle in the preindustrial atmosphere, with peak changes to particle concentrations in summer, probably due to the dominance of pure organic ion-induced NPF at this time of the year.

Our finding that CCN concentrations are relatively insensitive to the variation of ion concentrations over the solar cycle reflects the negative feedback whereby more nucleated particles compete for limited vapors, which reduces the probability of them growing to CCN size. While still very small, the effects of the solar cycle in both present-day and preindustrial conditions are substantially larger (by a factor 5–10) than those found by *Pierce and Adams* [2009b], even though the change in our NPF rate is smaller than in their "IONLIMIT" simulation, in which every ion produced nucleates a particle. This may be due to different estimates of vapor or primary particle emissions between the models. Our simulations do, however, seem broadly consistent with those of *Yu and Luo* [2014a], who see changes of around 0.4% in lower troposphere CCN0.2% concentrations, and the slightly higher change of 1.4% in N_3.

In our model, ternary NPF of sulfuric acid and organic vapors together ($J_{SA\text{-}org}$ in equation (3)) does not depend explicitly on the ion concentration because we have insufficient experimental data to parametrize this. Instead, a fixed fraction of this NPF pathway is assumed to be ion induced [*Dunne et al.*, 2016]. To calculate the potential importance of the solar cycle to $J_{SA\text{-}org}$, we assume the NPF rate scales with the ion concentration like the rate in the other ion-induced NPF pathways and redo the calculation described above. Typical ion concentrations in the CLOUD chamber I_{CLOUD} are of the order 500 ion pairs per cubic centimeter [*Franchin et al.*, 2015]. To set an upper limit, we assume that this organic NPF is all ion induced and replace $J_{SA\text{-}org}$ in our model by $J_{SA\text{-}org\text{-}ion}$, where

$$J_{SA\text{-}org\text{-}ion} = J_{SA\text{-}org}\frac{I}{I_{CLOUD}} \tag{10}$$

where I is our modeled ion pair concentration. When we do this, we find that over the solar cycle the change in CCN0.2% concentrations increases only slightly, to 0.5% in preindustrial and 0.4% in present-day conditions.

9. Importance of BVOCs for New Particle Formation and CCN

Similar techniques allow us to quantify the importance of biogenic volatile organic compounds (BVOCs) to CCN number concentrations in our model. It is important to revise these estimates given the increased importance of organics in our new NPF parametrizations, since secondary organic aerosol has been calculated to influence both direct [e.g., *Chung and Seinfeld*, 2002] and indirect [*Chuang et al.*, 2002] radiative forcing for well over a decade [*Kanakidou et al.*, 2005]. There is also much recent work in this area; for example, detailed estimates of the effect of changes to secondary organic aerosol on CCN and/or cloud droplet number formation over the historical period with the GEOS-chem [*D'Andrea et al.*, 2015], GLOMAP [*Scott et al.*, 2015], and ECHAM [*Makkonen et al.*, 2012] models.

As stated in section 7, 51% of present-day new particle formation and 86% of preindustrial NPF below 5.8 km altitude involves organic molecules. With zero organic vapors in our model, present-day cloud-level CCN0.2% concentrations are 26% lower than those when organic vapors are switched on. This estimate is within the range given in Table 2 of *Scott et al.* [2014]. In the preindustrial atmosphere, CCN concentrations are 41% lower without BVOCs. These estimates indicate the importance of BVOCs in CCN formation even when direct feedbacks are included: when BVOCs are removed, the condensation sink is reduced so the NPF rates of other compounds increase. The role of BVOCs varies regionally as shown in Figure 9.

An alternative estimate for the fraction of CCN that results from NPF involving BVOCs is obtained by multiplying the change in low-cloud-level CCN when NPF is included in the model by the fraction of NPF at CCN-forming altitudes (within 5.8 km of the surface) that is organic. We find that BVOCs are responsible for 27% of low-cloud-level CCN0.2% formation in the present-day atmosphere and 58% of CCN0.2% formation in the preindustrial atmosphere. The close agreement with the change to CCN concentration when BVOCs are removed in the present-day case is probably a coincidence. As with the case of ions (previous section) this is an estimate of the "real" role of BVOCs in CCN formation, without considering the direct feedback. However, this estimate will be biased toward regions where NPF rates are high, which may not necessarily be where CCN formation is efficient [*Pierce and Adams*, 2007].

To estimate the role of organic-mediated NPF and growth in forming CCN we remove only the highly oxygenated molecules (HOMs) that nucleate and grow particles to 3 nm in size but do not grow particles further from our model. When we do this, we find CCN0.2% concentrations decrease by 18% in the present-day and 32% in the preindustrial atmospheres. As these numbers are quite similar to the 26% and 41% calculated by removing all BVOCs, we conclude that the role of organics in aerosol formation is most important for the smallest particles, and of secondary importance for larger particles. We also know that only HOMs, whose saturation concentration C^* is usually well below 1 μgm^{-3}, can condense onto particles smaller than 3 nm diameter [*Tröstl et al.*, 2016]. Crudely, these statements imply that three quarters of the climate effect of BVOCs originates from HOMs. However, we do not simulate the volatility of the organic aerosol in our model, nor do we include secondary organic aerosol from isoprene or sesquiterpenes, so further work is needed to ensure these conclusions are robust.

The sensitivity of our model to perturbations in BVOC emissions was tested by doubling and halving the monoterpene emissions, motivated by the diversity in the inventories (see, for example, Figure 14 of *Sindelarova et al.* [2014]). When monoterpene emissions are doubled, low-cloud-level CCN0.2% concentrations increase by 10% in the present-day atmosphere and 16% in the preindustrial atmosphere (compared to the model run with the best estimate for the emissions). When they are halved, this CCN concentration decreases by 7.4% in the present-day atmosphere and by 12% in the preindustrial. The overall uncertainty on CCN due to BVOCs is probably larger than these numbers suggest as uncertain monoterpene emissions are not the only source of error. Other uncertainties stem from the use of a single proxy compound and the resultant assumptions, for example, that the reaction rates of all compounds are well represented by those of this proxy. The uncertainty is also larger than that which can be inferred from the perturbed parameter ensemble of *Lee et al.* [2013]. In their study, only sulfuric acid participated in NPF. Therefore, increasing BVOCs led to larger particles that activate more easily and also increased the coagulation sink, suppressing formation of new particles. Overall, the sensitivity of CCN concentrations to BVOC concentrations was therefore relatively small. Now, increasing BVOCs enhances new particle formation as well as condensation, and the sensitivity of CCN number to BVOC emissions is correspondingly larger.

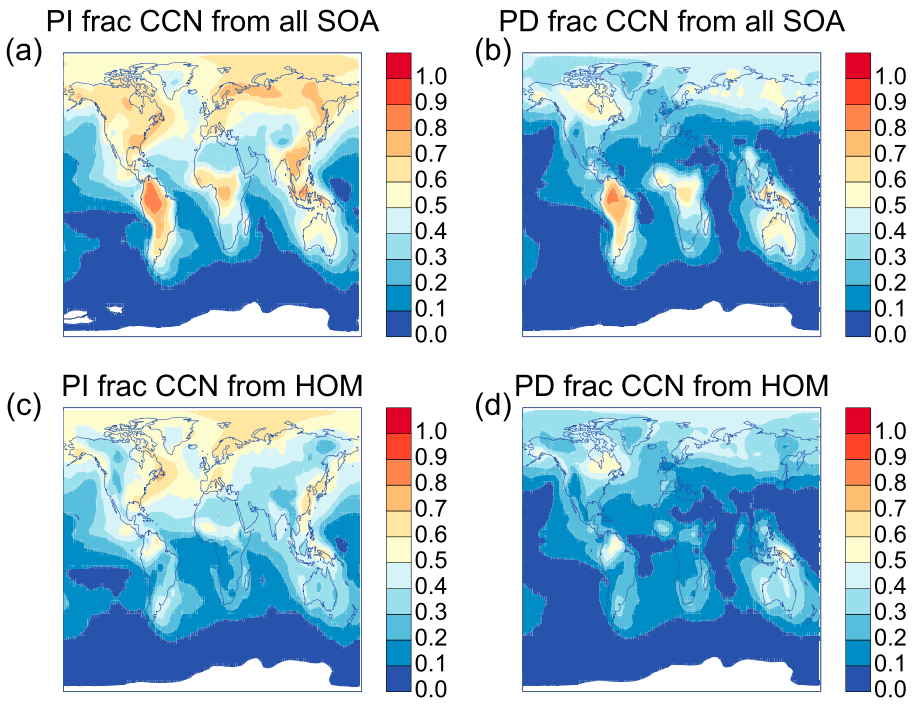

Figure 9. Annually averaged fractions of CCN0.2% concentrations at low cloud level (approximately 460–1100 m altitude) that result from (a, b) all SOA, i.e., all organic vapors that can form or grow particles of all sizes, and (c, d) the most highly oxygenated molecules (HOMs) including BioOxOrg, i.e., all vapors that can form or condense onto particles of less than 3 nm in diameter. The fractions *f* are approximated by comparing CCN0.2% concentrations in simulations with SOA or HOM formation switched off to the standard model runs, for example, $f_{SOA} = 1 - \frac{[CCN0.2\%(no\ SOA)]}{[CCN0.2\%(with\ SOA)]}$.

10. Conclusions

Our results suggest that slightly more than half of cloud-forming atmospheric particles originate from gas-to-particle conversion in the present-day atmosphere, and around two thirds in the preindustrial atmosphere. These fractions are calculated assuming that the fraction of CCN from NPF is equal to the relative change in CCN when NPF is included in our model. The estimated fraction depends on the time of year, the region of the planet considered, and the supersaturation of the cloud condensation nuclei. For example, in the Northern Hemisphere summer 69% of CCN1% in the present-day and 89% in the preindustrial atmospheres originate from NPF. This reflects the huge importance of the NPF of biogenic organics over unpolluted land masses in summer. On the other hand, in the Southern Hemisphere winter, more CCN originate from primary particles than from NPF, probably due to sea spray over oceans, and biomass burning in the Amazon dry season.

Our estimates of the role of NPF in present-day CCN formation are different from the previous estimate by *Merikanto et al.* [2009]. We also calculate a higher uncertainty range. In the present-day atmosphere we estimate 54% of CCN originate from NPF with an uncertainty range of 38–66%, while *Merikanto et al.* [2009] estimated 45%, with a range 31–49%. In the preindustrial atmosphere, our uncertainty range is larger still, at 44–84% with a best estimate of 68%.

Emissions of primary particles and vapors are most likely to dominate the uncertainties in our results, and we refer the reader to other work with the same model, for example, that of *Lee et al.* [2013], to evaluate the potential importance of other sources of error. Recent work to constrain the properties of primary emissions is therefore likely to be useful to future estimates. Some examples of studies of which we are aware but have not yet incorporated in our model include *Sakamoto et al.* [2016] for the biomass burning emissions diameter and parametrizations compared in, for example, *de Leeuw et al.* [2011] for sea spray. It will also be important to add potentially important aerosol sources to models not included before, such as the primary marine organic aerosol suggested by *Westervelt et al.* [2012].

Acknowledgments
We would like to thank CERN for supporting CLOUD with important technical and financial resources and for providing a particle beam from the CERN Proton Synchrotron. We also thank P. Carrie, L.-P. De Menezes, J. Dumollard, K. Ivanova, F. Josa, I. Krasin, R. Kristic, A. Laassiri, O.S. Maksumov, B. Marichy, H. Martinati, S.V. Mizin, R. Sitals, H.U. Walther, A. Wasem, and M. Wilhelmsson for their important contributions to the experiment. The computer modeling simulations were performed on ARC1 and ARC2, part of the High Performance Computing facilities at the University of Leeds, UK. This work also made use of the POLARIS facility of the N8 HPC Centre of Excellence, provided and funded by the N8 consortium and EPSRC (grant No.EP/K000225/1). The Centre is coordinated by the Universities of Leeds and Manchester. This research has received funding from the EC Seventh Framework Programme (Marie Curie Initial Training Networks "CLOUD-ITN" (215072) and "CLOUD-TRAIN" (316662), the FP7 EU Bacchus project under grant 603445-BACCHUS, and the Horizon 2020 projects CRESCENDO under grant agreement 641816 and the Marie-Sklodowska-Curie project nano-CAVa 656994), ERC-Starting MOCAPAF grant 57360 and ERC Advanced "ATMNUCLE" grant 227463, the German Federal Ministry of Education and Research (projects 01LK0902A and 01LK1222A), the Swiss National Science Foundation (projects 200020_135307 and 206620_141278), the Academy of Finland (Center of Excellence project 1118615 and other projects 135054, 133872, 251427, 139656, 139995, 137749, 141217, 141451, 138951, and 299574), the Finnish Funding Agency for Technology and Innovation, the V.is.l. Foundation, the Nessling Foundation, ERC Consolidator grant "NANODYNAMITE," 616075, the Portuguese Foundation for Science and Technology (project CERN/FP/116387/2010), the Swedish Research Council, Vetenskapsrådet (grant 2011-5120), the Presidium of the Russian Academy of Sciences and Russian Foundation for Basic Research (grants 08-02-91006-CERN and 12-02-91522-CERN), the U.S. National Science Foundation (grants AGS1136479, AGS1447056, AGS1439551, and CHE1012293), the U.S. Department of Energy (grant DE-SC0014469), the Davidow Foundation, and the NERC GASSP project under grant NE/J024252/1. We acknowledge financial support from the Royal Society Wolfson Merit Award. The simulation data presented in this manuscript

Fully incorporating the ion-induced NPF of biogenic organic molecules with ion-induced inorganic NPF has allowed us to update estimates of the possible role of ions in CCN formation, and of the solar cycle in modulating CCN. We estimate that 27% of low-cloud-level CCN0.2% in the present-day atmosphere and 40% in the preindustrial atmosphere originate from ion-induced NPF. Despite the important role of ions in CCN formation, our results, in agreement with previous work, suggest that solar cycle variations of ion concentration lead to a maximum 1% variation of CCN0.2% concentrations. This is insignificant on an 11 year timescale compared with fluctuations due to, for example, the El Niño–Southern Oscillation, variations in wildfires, or volcanoes. On multidecadal time scales, perhaps the cumulative effect of continually higher average ion concentrations could lead to a very small radiative forcing of climate. For example, at the time of the Maunder Minimum ion concentrations were higher on average by a comparable amount to the solar cycle amplitude for close to a century. However, these effects would be extremely difficult to disentangle from other, potentially much larger, sources of long-term variability such as changes to vegetation, solar irradiance, or volcanic activity. Our results must be qualified because we do not explicitly model aerosol-cloud interactions, and we assume NPF occurs over scales comparable to, or greater than, our low model resolution.

NPF also strongly affects the role of BVOCs in CCN formation [*Scott et al.*, 2014]. Almost all CCN formed over land at or below low cloud level probably contain a substantial fraction of BVOC molecules [*Jimenez et al.*, 2009]. We update previous studies with the latest NPF mechanisms and estimate that CCN0.2% concentrations would be 26% lower without BVOCs in the present-day atmosphere and 41% lower in the preindustrial atmosphere. The highly oxygenated molecules from BVOCs that contribute to NPF and growth of sub-3 nm aerosol particles are especially important; without these, preindustrial CCN0.2% concentrations would already be 30% lower.

The same perturbations to the emissions of aerosols and their precursors in our model have a greater effect on the role of NPF in CCN formation in the preindustrial atmosphere than in the present-day atmosphere. This is clear because the 40% uncertainty in the fraction of CCN that originates from NPF in the preindustrial atmosphere is larger than the 27% uncertainty in the present-day atmosphere. This reinforces the conclusion of *Carslaw et al.* [2013] that preindustrial aerosol concentrations were more sensitive to changes in emissions than they are today. Additionally, the preindustrial climate was more sensitive to aerosol, because aerosol concentrations were lower, and therefore, preindustrial clouds were more responsive to changes in aerosols [e.g., *Rosenfeld et al.*, 2008].

Both NPF and primary emissions are important throughout the present-day and preindustrial lower atmospheres, where aerosols influence climate most strongly. Aerosol number concentrations are especially sensitive to variations in primary emissions, because there are not fast feedbacks as in the case of variations of NPF. However, NPF is still responsible for the majority of CCN formation, and the role of compounds other than sulfuric acid, and the role of ions, in NPF cannot be ignored if realistic models of atmospheric aerosol are to be achieved.

References

Acosta Navarro, J. C., S. Smolander, H. Struthers, E. Zorita, A. M. Ekman, J. Kaplan, A. Guenther, A. Arneth, and I. Riipinen (2014), Global emissions of terpenoid VOCs from terrestrial vegetation in the last millennium, *J. Geophys. Res. Atmos.*, *119*, 6867–6885, doi:10.1002/2013JD021238.

Almeida, J., et al. (2013), Molecular understanding of sulphuric acid-amine particle nucleation in the atmosphere, *Nature*, *502*(7471), 359–363.

Benduhn, F., G. W. Mann, K. J. Pringle, D. O. Topping, G. McFiggans, and K. S. Carslaw (2016), Size-resolved simulations of the aerosol inorganic composition with the new hybrid dissolution solver HyDiS-1.0: Description, evaluation and first global modelling results, *Geosci. Model Dev.*, *9*(11), 3875–3906, doi:10.5194/gmd-9-3875-2016.

Benson, D., J. Yu, A. Markovich, and S.-H. Lee (2011), Ternary homogeneous nucleation of H_2SO_4, NH_3, and H_2O under conditions relevant to the lower troposphere, *Atmos. Chem. Phys.*, *11*(10), 4755–4766.

Bianchi, F., et al. (2016), New particle formation in the free troposphere: A question of chemistry and timing, *Science*, *352*(6289), 1109–1112.

Carslaw, K. S., et al. (2013), Large contribution of natural aerosols to uncertainty in indirect forcing, *Nature*, *503*(7474), 67–71.

Carslaw, K. S., H. Gordon, D. S. Hamilton, J. S. Johnson, L. A. Regayre, M. Yoshioka, and K. J. Pringle (2017), Aerosols in the pre-industrial atmosphere, *Curr. Clim. Change Rep.*, *3*, 1–15, doi:10.1007/s40641-017-0061-2.

Chen, M., M. Titcombe, J. Jiang, C. Jen, C. Kuang, M. L. Fischer, F. L. Eisele, J. I. Siepmann, D. R. Hanson, J. Zhao, and P. H. McMurry (2012), Acid–base chemical reaction model for nucleation rates in the polluted atmospheric boundary layer, *Proc. Natl. Acad. Sci. U.S.A.*, *109*(46), 18,713–18,718, doi:10.1073/pnas.1210285109.

Chipperfield, M. P. (2006), New version of the TOMCAT/SLIMCAT off-line chemical transport model: Intercomparison of stratospheric tracer experiments, *Q. J. R. Meteorol. Soc.*, *132*(617), 1179–1203, doi:10.1256/qj.05.51.

Chuang, C. C., J. E. Penner, J. M. Prospero, K. E. Grant, G. H. Rau, and K. Kawamoto (2002), Cloud susceptibility and the first aerosol indirect forcing: Sensitivity to black carbon and aerosol concentrations, *J. Geophys. Res. Atmos.*, *107*(D21), 4564, doi:10.1029/2000JD000215.

are available from Zenodo at DOI 10.5281/zenodo.821582. The full NPF parametrizations used, and summaries of the model results, are provided in the supporting information.

Chung, S. H., and J. H. Seinfeld (2002), Global distribution and climate forcing of carbonaceous aerosols, *J. Geophys. Res.*, *107*(D19), 4407, doi:10.1029/2001JD001397.

Crounse, J. D., L. B. Nielsen, S. Jørgensen, H. G. Kjaergaard, and P. O. Wennberg (2013), Autoxidation of organic compounds in the atmosphere, *J. Phys. Chem. Lett.*, *4*(20), 3513–3520.

D'Andrea, S. D., J. C. Acosta Navarro, S. C. Farina, C. E. Scott, A. Rap, D. K. Farmer, D. V. Spracklen, I. Riipinen, and J. R. Pierce (2015), Aerosol size distribution and radiative forcing response to anthropogenically driven historical changes in biogenic secondary organic aerosol formation, *Atmos. Chem. Phys.*, *15*(5), 2247–2268, doi:10.5194/acp-15-2247-2015.

de Leeuw, G., E. L. Andreas, M. D. Anguelova, C. W. Fairall, E. R. Lewis, C. O'Dowd, M. Schulz, and S. E. Schwartz (2011), Production flux of sea spray aerosol, *Rev. Geophys.*, *49*, RG2001, doi:10.1029/2010RG000349.

Dentener, F., et al. (2006), Emissions of primary aerosol and precursor gases in the years 2000 and 1750 prescribed data-sets for AeroCom, *Atmos. Chem. Phys.*, *6*(12), 4321–4344, doi:10.5194/acp-6-4321-2006.

Dunne, E., L. Lee, C. Reddington, and K. Carslaw (2012), No statistically significant effect of a short-term decrease in the nucleation rate on atmospheric aerosols, *Atmos. Chem. Phys.*, *12*(23), 11,573–11,587.

Dunne, E. M., et al. (2016), Global atmospheric particle formation from CERN CLOUD measurements, *Science*, *354*, 1119–1124, doi:10.1126/science.aaf2649.

Duplissy, J., et al. (2016), Effect of ions on sulfuric acid-water binary particle formation: 2. Experimental data and comparison with QC-normalized classical nucleation theory, *J. Geophys. Res. Atmos.*, *121*, 1752–1775, doi:10.1002/2015JD023539.

Ehn, M., et al. (2014), A large source of low-volatility secondary organic aerosol, *Nature*, *506*(7489), 476–479.

Finlay, C. C., et al. (2010), International geomagnetic reference field: The eleventh generation, *Geophys. J. Int.*, *183*(3), 1216–1230, doi:10.1111/j.1365-246X.2010.04804.x.

Franchin, A., et al. (2015), Experimental investigation of ion–ion recombination under atmospheric conditions, *Atmos. Chem. Phys.*, *15*(13), 7203–7216, doi:10.5194/acp-15-7203-2015.

Fraser-Smith, A. C. (1987), Centered and eccentric geomagnetic dipoles and their poles, 1600–1985, *Rev. Geophys.*, *25*(1), 1–16, doi:10.1029/RG025i001p00001.

Gong, S. L. (2003), A parameterization of sea-salt aerosol source function for sub- and super-micron particles, *Global Biogeochem. Cycles*, *17*(4), 1097, doi:10.1029/2003GB002079.

Gordon, H., et al. (2016), Reduced anthropogenic aerosol radiative forcing caused by biogenic new particle formation, *Proc. Natl. Acad. Sci. U.S.A.*, *113*, 12053–12058, doi:10.1073/pnas.1602360113.

Heald, C. L., and D. V. Spracklen (2015), Land use change impacts on air quality and climate, *Chem. Rev.*, *115*(10), 4476–4496, doi:10.1021/cr500446g.

Iida, K., M. R. Stolzenburg, and P. H. McMurry (2009), Effect of working fluid on sub-2 nm particle detection with a laminar flow ultrafine condensation particle counter, *Aerosol Sci. Technol.*, *43*(1), 81–96, doi:10.1080/02786820802488194.

Jen, C. N., P. H. McMurry, and D. R. Hanson (2014), Stabilization of sulfuric acid dimers by ammonia, methylamine, dimethylamine, and trimethylamine, *J. Geophys. Res. Atmos.*, *119*, 7502–7514, doi:10.1002/2014JD021592.

Jimenez, J. L., et al. (2009), Evolution of organic aerosols in the atmosphere, *Science*, *326*(5959), 1525–1529.

Jokinen, T., et al. (2015), Production of extremely low volatile organic compounds from biogenic emissions: Measured yields and atmospheric implications, *Proc. Natl. Acad. Sci. U.S.A.*, *112*(23), 7123–7128, doi:10.1073/pnas.1423977112.

Jones, A., D. Roberts, and A. Slingo (1994), A climate model study of indirect radiative forcing, *Nature*, *370*, 450–453.

Junninen, H., et al. (2010), A high-resolution mass spectrometer to measure atmospheric ion composition, *Atmos. Meas. Tech.*, *3*(4), 1039–1053, doi:10.5194/amt-3-1039-2010.

Kanakidou, M., et al. (2005), Organic aerosol and global climate modelling: A review, *Atmos. Chem. Phys.*, *5*(4), 1053–1123, doi:10.5194/acp-5-1053-2005.

Kazil, J., et al. (2010), Aerosol nucleation and its role for clouds and Earth's radiative forcing in the aerosol-climate model ECHAM5-HAM, *Atmos. Chem. Phys.*, *10*(22), 10,733–10,752.

Kazil, J., K. Zhang, P. Stier, J. Feichter, U. Lohmann, and K. O'Brien (2012), The present-day decadal solar cycle modulation of Earth's radiative forcing via charged H_2SO_4/H_2O aerosol nucleation, *Geophys. Res. Lett.*, *39*, L02805, doi:10.1029/2011GL050058.

Kerminen, V.-M., and M. Kulmala (2002), Analytical formulae connecting the "real" and the "apparent" nucleation rate and the nuclei number concentration for atmospheric nucleation events, *J. Aerosol Sci.*, *33*(4), 609–622.

Kettle, A. J., and M. O. Andreae (2000), Flux of dimethylsulfide from the oceans: A comparison of updated data sets and flux models, *J. Geophys. Res.*, *105*(D22), 26,793–26,808.

Kirkby, J., et al. (2016), Ion-induced nucleation of pure biogenic particles, *Nature*, *533*(7604), 521–526.

Kontkanen, J., et al. (2017), Measurements of sub-3 nm particles using a particle size magnifier in different environments: From clean mountain top to polluted megacities, *Atmos. Chem. Phys.*, *17*(3), 2163–2187, doi:10.5194/acp-17-2163-2017.

Kulmala, M., K. E. J. Lehtinen, and A. Laaksonen (2006), Cluster activation theory as an explanation of the linear dependence between formation rate of 3 nm particles and sulphuric acid concentration, *Atmos. Chem. Phys.*, *6*(3), 787–793, doi:10.5194/acp-6-787-2006.

Kürten, A., et al. (2016), Experimental particle formation rates spanning tropospheric sulfuric acid and ammonia abundances, ion production rates, and temperatures, *J. Geophys. Res. Atmos.*, *121*, 12,377–12,400, doi:10.1002/2015JD023908.

Lee, L. A., K. J. Pringle, C. L. Reddington, G. W. Mann, P. Stier, D. V. Spracklen, J. R. Pierce, and K. S. Carslaw (2013), The magnitude and causes of uncertainty in global model simulations of cloud condensation nuclei, *Atmos. Chem. Phys.*, *13*(17), 8879–8914, doi:10.5194/acp-13-8879-2013.

Luo, G., and F. Yu (2011), Sensitivity of global cloud condensation nuclei concentrations to primary sulfate emission parameterizations, *Atmos. Chem. Phys.*, *11*(5), 1949–1959, doi:10.5194/acp-11-1949-2011.

Makkonen, R., et al. (2009), Sensitivity of aerosol concentrations and cloud properties to nucleation and secondary organic distribution in ECHAM5-HAM global circulation model, *Atmos. Chem. Phys.*, *9*(5), 1747–1766, doi:10.5194/acp-9-1747-2009.

Makkonen, R., A. Asmi, V.-M. Kerminen, M. Boy, A. Arneth, A. Guenther, and M. Kulmala (2012), BVOC-aerosol-climate interactions in the global aerosol-climate model ECHAM5.5-HAM2, *Atmos. Chem. Phys.*, *12*(21), 10,077–10,096, doi:10.5194/acp-12-10077-2012.

Manktelow, P. T., K. S. Carslaw, G. W. Mann, and D. V. Spracklen (2009), Variable CCN formation potential of regional sulfur emissions, *Atmos. Chem. Phys.*, *9*(10), 3253–3259.

Mann, G. W., K. S. Carslaw, D. V. Spracklen, D. A. Ridley, P. T. Manktelow, M. P. Chipperfield, S. J. Pickering, and C. E. Johnson (2010), Description and evaluation of GLOMAP-mode: A modal global aerosol microphysics model for the UKCA composition-climate model, *Geosci. Model Dev.*, *3*(2), 519–551.

Mann, G. W., et al. (2012), Intercomparison of modal and sectional aerosol microphysics representations within the same 3-D global chemical transport model, *Atmos. Chem. Phys.*, *12*(10), 4449–4476, doi:10.5194/acp-12-4449-2012.

Mårtensson, E., E. Nilsson, G. de Leeuw, L. Cohen, and H.-C. Hansson (2003), Laboratory simulations and parameterization of the primary marine aerosol production, *J. Geophys. Res.*, *108*(D9), 4297, doi:10.1029/2002JD002263.
Merikanto, J., D. V. Spracklen, G. W. Mann, S. J. Pickering, and K. S. Carslaw (2009), Impact of nucleation on global CCN, *Atmos. Chem. Phys.*, *9*(21), 8601–8616, doi:10.5194/acp-9-8601-2009.
Merikanto, J., D. V. Spracklen, K. J. Pringle, and K. S. Carslaw (2010), Effects of boundary layer particle formation on cloud droplet number and changes in cloud albedo from 1850 to 2000, *Atmos. Chem. Phys.*, *10*(2), 695–705.
Metzger, A., et al. (2010), Evidence for the role of organics in aerosol particle formation under atmospheric conditions, *Proc. Natl. Acad. Sci. U.S.A.*, *107*, 6646–6651, doi:10.1073/pnas.0911330107.
Monahan, E. C., D. E. Spiel, and K. L. Davidson (1986), A model of marine aerosol generation via whitecaps and wave disruption, in *Oceanic Whitecaps*, edited by E. C. Monahan and G. M. Niocaill, pp. 167–174, Springer, Netherlands.
Nieminen, T., K. E. J. Lehtinen, and M. Kulmala (2010), Sub-10 nm particle growth by vapor condensation effects of vapor molecule size and particle thermal speed, *Atmos. Chem. Phys.*, *10*(20), 9773–9779, doi:10.5194/acp-10-9773-2010.
Petters, M. D., and S. M. Kreidenweis (2007), A single parameter representation of hygroscopic growth and cloud condensation nucleus activity, *Atmos. Chem. Phys.*, *7*(8), 1961–1971, doi:10.5194/acp-7-1961-2007.
Pierce, J. R., and P. J. Adams (2007), Efficiency of cloud condensation nuclei formation from ultrafine particles, *Atmos. Chem. Phys.*, *7*(5), 1367–1379.
Pierce, J. R., and P. J. Adams (2009a), Uncertainty in global CCN concentrations from uncertain aerosol nucleation and primary emission rates, *Atmos. Chem. Phys.*, *9*(4), 1339–1356, doi:10.5194/acp-9-1339-2009.
Pierce, J. R., and P. J. Adams (2009b), Can cosmic rays affect cloud condensation nuclei by altering new particle formation rates?, *Geophys. Res. Lett.*, *36*, L09820, doi:10.1029/2009GL037946.
Riccobono, F., et al. (2014), Oxidation products of biogenic emissions contribute to nucleation of atmospheric particles, *Science*, *344*(6185), 717–721, doi:10.1126/science.1243527.
Rosenfeld, D., U. Lohmann, G. B. Raga, C. D. O'Dowd, M. Kulmala, S. Fuzzi, A. Reissell, and M. O. Andreae (2008), Flood or drought: How do aerosols affect precipitation?, *Science*, *321*(5894), 1309–1313.
Sakamoto, K. M., J. R. Laing, R. G. Stevens, D. A. Jaffe, and J. R. Pierce (2016), The evolution of biomass-burning aerosol size distributions due to coagulation: Dependence on fire and meteorological details and parameterization, *Atmos. Chem. Phys.*, *16*(12), 7709–7724, doi:10.5194/acp-16-7709-2016.
Schobesberger, S., et al. (2013), Molecular understanding of atmospheric particle formation from sulfuric acid and large oxidized organic molecules, *Proc. Natl. Acad. Sci. U.S.A.*, *110*(43), 17,223–17,228, doi:10.1073/pnas.1306973110.
Scott, C. E., et al. (2014), The direct and indirect radiative effects of biogenic secondary organic aerosol, *Atmos. Chem. Phys.*, *14*(1), 447–470, doi:10.5194/acp-14-447-2014.
Scott, C. E., et al. (2015), Impact of gas-to-particle partitioning approaches on the simulated radiative effects of biogenic secondary organic aerosol, *Atmos. Chem. Phys.*, *15*(22), 12,989–13,001, doi:10.5194/acp-15-12989-2015.
Sindelarova, K., C. Granier, I. Bouarar, A. Guenther, S. Tilmes, T. Stavrakou, J.-F. Müller, U. Kuhn, P. Stefani, and W. Knorr (2014), Global data set of biogenic VOC emissions calculated by the MEGAN model over the last 30 years, *Atmos. Chem. Phys.*, *14*(17), 9317–9341, doi:10.5194/acp-14-9317-2014.
Snow-Kropla, E. J., J. R. Pierce, D. M. Westervelt, and W. Trivitayanurak (2011), Cosmic rays, aerosol formation and cloud-condensation nuclei: Sensitivities to model uncertainties, *Atmos. Chem. Phys.*, *11*(8), 4001–4013, doi:10.5194/acp-11-4001-2011.
Spracklen, D. V., K. J. Pringle, K. S. Carslaw, M. P. Chipperfield, and G. W. Mann (2005), A global off-line model of size-resolved aerosol microphysics: I. Model development and prediction of aerosol properties, *Atmos. Chem. Phys.*, *5*(8), 2227–2252.
Spracklen, D. V., et al. (2008), Contribution of particle formation to global cloud condensation nuclei concentrations, *Geophys. Res. Lett.*, *35*, L06808, doi:10.1029/2007GL033038.
Stier, P., et al. (2005), The aerosol-climate model ECHAM5-HAM, *Atmos. Chem. Phys.*, *5*(4), 1125–1156.
Tröstl, J., et al. (2016), The role of low-volatility organic compounds in initial particle growth in the atmosphere, *Nature*, *533*(7604), 527–531. letter.
Usoskin, I. G., K. Alanko-Huotari, G. A. Kovaltsov, and K. Mursula (2005), Heliospheric modulation of cosmic rays: Monthly reconstruction for 1951–2004, *J. Geophys. Res.*, *110*, A12108, doi:10.1029/2005JA011250.
Usoskin, I. G., G. A. Bazilevskaya, and G. A. Kovaltsov (2011), Solar modulation parameter for cosmic rays since 1936 reconstructed from ground-based neutron monitors and ionization chambers, *J. Geophys. Res.*, *116*, A02104, doi:10.1029/2010JA016105.
Usoskin, I. G., et al. (2015), The Maunder minimum (1645–1715) was indeed a grand minimum: A reassessment of multiple datasets, *Astron. Astrophys.*, *581*, A95.
Van Der Werf, G. R., J. T. Randerson, G. J. Collatz, and L. Giglio (2003), Carbon emissions from fires in tropical and subtropical ecosystems, *Global Change Biol.*, *9*(4), 547–562, doi:10.1046/j.1365-2486.2003.00604.x.
Vanhanen, J., J. Mikkilä, K. Lehtipalo, M. Sipilä, H. Manninen, E. Siivola, T. Petäjä, and M. Kulmala (2011), Particle size magnifier for nano-CN detection, *Aerosol Sci. Technol.*, *45*(4), 533–542.
Wang, M., and J. E. Penner (2009), Aerosol indirect forcing in a global model with particle nucleation, *Atmos. Chem. Phys.*, *9*(1), 239–260, doi:10.5194/acp-9-239-2009.
Westervelt, D. M., R. H. Moore, A. Nenes, and P. J. Adams (2012), Effect of primary organic sea spray emissions on cloud condensation nuclei concentrations, *Atmos. Chem. Phys.*, *12*(1), 89–101, doi:10.5194/acp-12-89-2012.
Westervelt, D. M., J. R. Pierce, and P. J. Adams (2014), Analysis of feedbacks between nucleation rate, survival probability and cloud condensation nuclei formation, *Atmos. Chem. Phys.*, *14*(11), 5577–5597, doi:10.5194/acp-14-5577-2014.
Wyche, K. P., R. Blake, A. M. Ellis, P. S. Monks, T. Brauers, R. Koppmann, and E. Apel (2007), Technical note: Performance of Chemical Ionization Reaction Time-of-Flight Mass Spectrometry (CIR-TOF-MS) for the measurement of atmospherically significant oxygenated volatile organic compounds, *Atmos. Chem. Phys.*, *7*(3), 609–620.
Yu, F., and G. Luo (2009), Simulation of particle size distribution with a global aerosol model: Contribution of nucleation to aerosol and CCN number concentrations, *Atmos. Chem. Phys.*, *9*(20), 7691–7710.
Yu, F., and G. Luo (2014a), Effect of solar variations on particle formation and cloud condensation nuclei, *Environ. Res. Lett.*, *9*(4), 045004.
Yu, F., and G. Luo (2014b), Modeling of gaseous methylamines in the global atmosphere: Impacts of oxidation and aerosol uptake, *Atmos. Chem. Phys.*, *14*(22), 12,455–12,464, doi:10.5194/acp-14-12455-2014.
Yu, F., G. Luo, X. Liu, R. C. Easter, X. Ma, and S. J. Ghan (2012), Indirect radiative forcing by ion-mediated nucleation of aerosol, *Atmos. Chem. Phys.*, *12*(23), 11,451–11,463, doi:10.5194/acp-12-11451-2012.

Yu, F., G. Luo, A. B. Nadykto, and J. Herb (2016), Impact of temperature dependence on the possible contribution of organics to new particle formation in the atmosphere, *Atmos. Chem. Phys. Discuss.*, *2016*, 1–22, doi:10.5194/acp-2016-812.

Zhang, K., et al. (2011), Radon activity in the lower troposphere and its impact on ionization rate: A global estimate using different radon emissions, *Atmos. Chem. Phys.*, *11*(15), 7817–7838, doi:10.5194/acp-11-7817-2011.

Zollner, J. H., W. A. Glasoe, B. Panta, K. K. Carlson, P. H. McMurry, and D. R. Hanson (2012), Sulfuric acid nucleation: Power dependencies, variation with relative humidity, and effect of bases, *Atmos. Chem. Phys.*, *12*(10), 4399–4411, doi:10.5194/acp-12-4399-2012.